Effect of radiolysis on container materials degradation in a spent fuel dry cask storage environment

by

Dennis Wayne Vinson

A Thesis Submitted to the

Graduate Faculty in Partial Fulfillment of the

Requirements for the Degree of

MASTER OF SCIENCE

Department: Mechanical Engineering
Major: Nuclear Engineering

Signatures have been redacted for privacy

Signatures have been redacted for privacy

Iowa State University
Ames, Iowa

1995

This work is dedicated to my fiancee, Jessica;
without her personal sacrifice
and endless support and encouragement
this goal would not have been realized.

TABLE OF CONTENTS

CHAPTER 1. INTRODUCTION

Federal Legislation of High-Level Radioactive Waste

In an attempt to close the nuclear fuel cycle and dispose of the growing volume of high-level radioactive waste, the 97th United States Congress enacted the Nuclear Waste Policy Act of 1982 (NWPA) [1]. The NWPA was amended in 1987 by the Nuclear Waste Policy Amendment Act (NWPAA) [2]. A summary of the NWPA and the NWPAA is provided herein.

The NWPA delegated the responsibility for final disposal of high-level radioactive waste to the federal government, specifically the Department of Energy (DOE). The NWPA set specific goals for DOE to achieve and specific times in which to reach them. In addition, the DOE Office of Civilian Radioactive Waste Management (OCRWM) was established with the responsibility of complying with the new time line. The federal government was made responsible for construction and licensing of repositories and interim storage facilities. The OCRWM was required to provide for the initiation of deep geological disposal of commercial spent nuclear fuel and high-level radioactive waste by 31 January, 1998 [3].

The individual generators and owners of high-level radioactive waste, however, were found responsible for shouldering the financial burden incurred in the waste disposal. These costs include those incurred for interim storage and temporary onsite storage. To achieve this end, the Nuclear Waste Fund was established by the NWPA, to be composed of payments made by the generators and owners of spent fuel and other high-level radioactive waste. The NWPAA limited the site characterization to only the Yucca Mountain site in Nevada [3]. In

addition, the NWPAA extended the deadlines imposed on the OCRWM by the NWPA by about 5 years. Figure 1.1 shows a timeline for proposed milestones set by the NWPAA.

DOE is currently responsible for accepting commercial spent nuclear fuel and high-level radioactive waste by 31 January, 1998. In an attempt to meet this goal, DOE completed a plan for a monitored retrievable storage facility (MRS) for long-term storage of spent fuel, as prescribed by the NWPA. The DOE proposal, completed in 1986, called for a MRS to be sited at Oak Ridge. However, the NWPAA nullified the proposal and set up an MRS Review Commission to evaluate the need for such a facility [3].

Even with all of the attention and money that high-level waste has generated, it is unlikely that the federal government will be able to meet its obligations. With the deadline for acceptance of spent fuel from this countries operating nuclear power plants less than three years away, DOE seems no closer to being able to fulfill these obligations than in 1982. This places the burden of spent fuel storage squarely on the shoulders of the utilities that operate nuclear power plants, and thus generate the bulk of the high-level waste. These utilities have a number of options for storage of their spent fuel, and the remainder of this chapter will address several of these options.

Spent Fuel Storage Options

Spent fuel storage options can be classified into two groups. Spent fuel can be stored in pools of water or they may be stored dry. Storage may be at the reactor site (AR) or away from the reactor site (AFR). The majority of the spent fuel in the United States has been in AR storage. As of 1992, only 2 AFR storage facilities were in operation. These were Morris

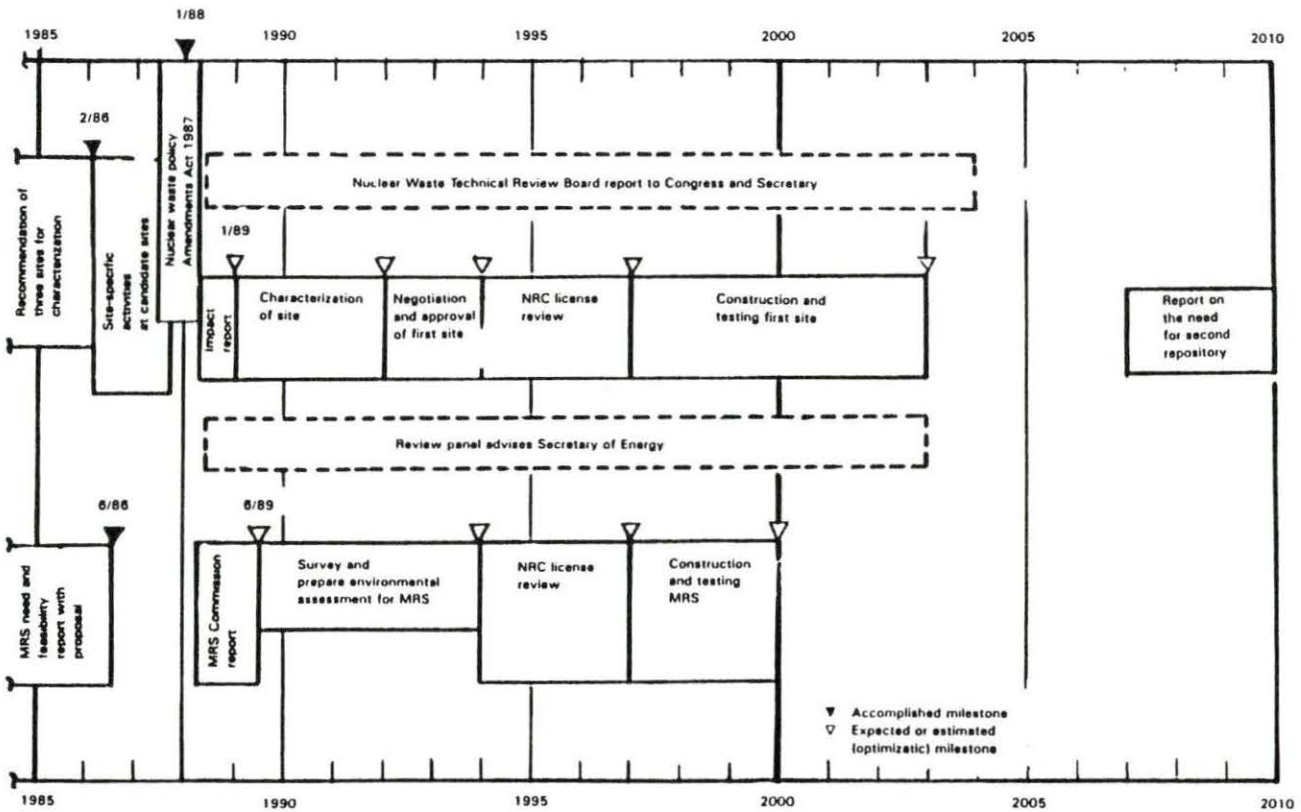

Figure 1.1. Proposed milestones for the design, construction, and operation of the MRS and the first geologic repository [3, p. 65].

Operation AFR Spent Fuel Storage Facility, operated by General Electric Company (GE), and a second AFR Spent Fuel Storage Facility, operated by West Valley Demonstration Project. In March of 1992, the West Valley Demonstration Project AFR storage facility had already reached capacity and the GE AFR storage facility had reached nearly 60% of its capacity [4]. Both of these are wet storage facilities.

Wet storage

"When commercial nuclear power plants were first built in the United States, the spent fuel pools were usually designed to hold [a number of fuel assemblies equivalent to about] two to three cores. [This was due to the fact that] the spent fuel was expected to be reprocessed within a few years of discharge" [3, p. 47]. To date, significant reprocessing of spent fuel has not occurred in this country. This is primarily due to the high costs associated with spent fuel reprocessing and the limited market for reprocessed fuel.

While DOE slowly progresses toward fulfilling its obligations with the nuclear utilities to accept spent fuel, the energy requirements in the United States continue to increase steadily. This means that utilities must continue to operate existing nuclear reactors, and thus, they continue to generate high-level radioactive waste, in the form of spent fuel. Therefore, the utilities must find ways to store the spent fuel. The most common form of spent fuel storage is AR storage in preexisting spent fuel pools. However, these spent fuel pools are rapidly reaching design capacity. There are a few options available to increase the storage capacity of onsite spent fuel pools.

The approach that requires the least development is the expansion of spent fuel pools. A utility may choose to either build a new pool or to expand an existing one. This method of increasing storage capacity, however, is relatively expensive.

A second method of increasing storage capacity is the reracking of spent fuel in an existing pool. "Partly because a need for large storage capacities was not foreseen and partly because the Nuclear Regulatory Commission (NRC) was conservative in its storage requirements, fuel was stored on 53 centimeter centers in the pools" [3, p. 58]. Experience in spent fuel storage and improved calculation techniques have shown that most utilities can increase storage by as much as 500% by reducing fuel spacing to 23 centimeter centers [3]. This increase is made possible by taking credit for the fact that the radioactive fuel has been exposed to a high neutron flux in the reactor, reducing the amount of fissile material in the fuel and increasing the inventory of neutron absorbing fission products. Also, the utilities can increase safety margins by placing neutron absorbers in the spent fuel pool. These absorbers may be in the form of boron additions to the pool water or by placing B_4C plates in the pools between spent fuel assemblies.

Other wet storage options that can delay the need for additional storage capacity are fuel consolidation and fuel transshipment. Fuel consolidation requires the disassembly of spent fuel rods and the subsequent rearrangement of the fuel rods into a close-packed geometry in a storage canister. This method is relatively inexpensive for spent fuel pools that can support the added weight of the canisters. Transshipment is a term given to the process of shipping fuel from one spent fuel pool to another. Utilities could ship fuel from a reactor

with a relatively full spent fuel pool to a reactor with more available storage space. These two options have recently been licensed by the NRC. However, licensing can take considerable time [3]. Other obstacles to transshipment are state and local government regulations. Many state and local laws strictly prohibit transshipment.

Dry storage

The wet storage options discussed previously can only provide finite increases in storage capacity. In addition, wet storage requires relatively high maintenance and personnel costs, offers little flexibility, increases fuel handling requirements, and increases the risk of radiation exposure. The development of dry storage techniques for spent fuel addresses many of these issues.

Dry storage technology offers increased flexibility to specific sites. Dry storage eliminates the need for full time dedicated personnel and the risk of loss of coolant accidents. Also, dry storage facilities may be readily expanded. Many of the dry storage concepts are less expensive and more reliable than wet storage options. Increased reliability stems from the fact that many dry storage concepts are passively cooled, requiring no pumps or blowers.

Four dry storage concepts have been developed and deployed. These are vaults, subsurface dry caisson or drywells, spent fuel transport and storage casks, and silos or concrete canisters [5]. A brief summary of each of these concepts, as described by the International Atomic Energy Agency (IAEA) [5], is provided herein.

Vault storage -- This concept consists of a radiation resistant vault that is relatively simple in design. The vault is constructed of reinforced concrete. Partial burial of the vault

provides increased shielding. Facilities are required for receipt and handling of spent fuel assemblies. Decay heat produced by spent fuel within the vault may be removed by conduction or by convection; both of which may be provided by passive cooling systems. This storage concept provides capability for modular expansion. A vault storage design was initially licensed by the NRC in March 1988 [5].

Spent fuel transport and storage cask -- The spent fuel transport cask is an established technology. Their has been more than 30 years of service experience with spent fuel casks. Recently, efforts have been made to modify the transport cask for long-term storage. Several companies are presently developing transport/storage casks for dry storage of spent fuel [5].

Subsurface dry caisson or drywell -- This concept consists of spent fuel assemblies that are encapsulated and sealed in high integrity steel overpacks and stored underground in earth caissons. A caisson is a watertight chamber used in construction work as a foundation [6]. The caisson itself is constructed of corrugated pipe that is cathodically protected. The caisson is covered using a concrete shield plug. Decay heat removal in this design requires conduction through the earth surrounding the caisson and eventual convection to the atmosphere. This design is limited by maximum temperatures, moisture, and overpack corrosion [5].

Silos or concrete canister -- The Nutech Horizontal Modular Storage System (NUHOMS) manufactured by Nutech Engineers Inc. is the most widely used concrete storage system in the United States. At least three utilities have licensed NUHOMS modules for spent fuel storage. In this system, spent fuel is stored in a stainless steel canister filled with either

helium or nitrogen to inhibit oxidation of the spent fuel cladding [5]. Radiation shielding is provided by concrete modules. Decay heat is dissipated by conduction through the canister and natural convection through air channels in the concrete modules.

Most dry storage concepts employ atmospheric air for convective cooling of steel canisters. Though relative humidity varies with geographic region, atmospheric air always contains some water vapor. The mechanisms for corrosion of steel exposed to the atmosphere are pretty well established [7]. However, there has been little work completed in the area of corrosion in irradiated moist air environments. Recent research has suggested that even small amounts of water vapor in air can result in the production of significant quantities of nitric acid and other oxidizing products in the presence of a radiation field, as is expected at the surface of spent fuel containers [9-21].

It is expected that radiolysis will increase the corrosion rate of steel spent fuel containers. The objective of the present study is to quantify the increase in corrosion rate of spent fuel storage containers due to radiolysis. This research involves irradiating carbon steel in a moist air environment in an attempt to quantify the deleterious effects of radiolysis products on the long-term corrosion resistance of spent fuel containers. Experiments have been completed to evaluate the expected buffering effects of the concrete structure surrounding the spent fuel canisters. Also, the effects of radiolysis products on galvanic corrosion rates has been evaluated. Upon breaching the spent fuel container, or the corrosion allowance material in the case of permanent deep geological disposal, the predominant corrosion mechanism is expected to be galvanic in nature. It is expected that galvanic

corrosion may also be increased due to the radiolysis products produced in irradiated moist air environments.

CHAPTER 2. LITERATURE REVIEW

Corrosion Mechanisms

Fundamentals of corrosion

A summary of the fundamentals of general corrosion in candidate corrosion-allowance materials for deep geologic disposal containers has been completed by Vinson, et al [7]. Corrosion, or its scientific synonym, "oxidation" is an electrochemical reaction between two elements by which a metal loses an electron to another species taking part in the reaction. This species, usually oxygen, is reduced.

A metal oxide consists primarily of positively charged metal ions, Me^{z+}, where z is an integer, and larger, negatively charged oxygen ions, O^{2-}. Since the sum of the positive charges is equal to the sum of the negative charges, the overall oxide film is electrically neutral, although small regions can be either n-type or p-type semiconductors.

Oxides are predominantly ionic in character, although some covalent bonding may exist. There is a continuous transition from ionic to covalent bonding. Where a compound lies between the two types depends upon the difference between the electronegativity of atoms involved in the process. The electronegativity of an atom describes the tendency of that atom to ionize.

Oxidation of a metal results in a change in the free energy of the system. It is this change in free energy of the system that drives the electrochemical reactions involved in oxidation process. The change in free energy of the system is equal to the amount of work done or absorbed during the process minus the change in entropy of the system ($\Delta G=\Delta H-$

$T\Delta S$). In order for the oxidation reaction to occur, the reaction must cause a reduction in the free energy of the system. The standard free energy change for nearly all oxides is negative. This means that oxides are more thermodynamically stable in oxygen atmospheres than metals.

Since free energy changes are negative for the formation of metal oxides, all metals should revert to a combined, and therefore more stable, state when exposed to the atmosphere. It is due to the kinetics of oxidation reactions that this does not occur in times significant for the performance of engineering structures. The formation of a metal oxide on a bare metal surface usually restricts further access of one reactant to the other. When oxide thicknesses reach a certain value, 1-4 nm, oxide growth usually ceases. The oxide layer forms a protective barrier between the reacting metal and oxygen due to the continuous, non-porous nature of the layer that usually forms. In the event that the generated oxide layer is not continuous or is porous, the oxidation reaction continues and the metal will be converted to oxide. Thus, the very existence of metals and alloys is dependent on the ability of these materials to form protective oxide layers.

Initial stages of oxidation

Oxidation begins by a physical adsorption of oxygen molecules on the bare metal surface. These oxygen molecules then dissociate into atoms. At this point, oxygen atoms are dissolved in the metal. The atoms on the surface become much more strongly bound by a process of chemisorption that occurs with a much higher energy change, as high as 600 kJ/mol. This is up to 30 times as high as the energy of the adsorption process. There is experimental evidence that oxygen chemisorption is associated with the movement of a

specific number of metal atoms into the plane of the adsorbed oxygen atoms [7]. Together, the metal atoms and the adsorbed oxygen atoms form a very stable structure consisting of both positive and negative species that have been shown to be more stable than the bulk oxide. The transition of the monolayer to crystalline oxide must be explained by the effect of a second outer layer of chemisorbed oxygen molecules in altering the free energy balance so that the oxide becomes more stable than the monolayer.

Oxidation kinetics

Oxidation rates for low temperatures are usually described with reference to the mathematical relationship between oxide thickness and time by the following formulas.

$y = k_1 * \log(t)$ logarithmic

$1/y = k_2 - k_3 * \log(t)$ inverse logarithmic

$y = k_4 * (1 - \exp(-k_5 * t))$ asymptotic

for thin films, and

$y^2 = k_6 * t$ parabolic

$y = k_7$ rectilinear

for thicker films. The terms, k_i, are constants, and the oxide thickness, y, is assumed to be uniform.

For very thin films, there is a strong electric field across the oxide layer that causes metal ions to cross through the film. As the film gets thicker [1-4 nm], the electric field is no longer sufficient to maintain oxide growth. Unless there is sufficient thermal energy present to cause continued growth by ionic diffusion under an activity gradient in the film, the oxidation

rate will fall off rapidly. As long as oxide growth is dependent on the existence of electric fields, the oxide will never grow to significant thicknesses, even as oxidation temperature is increased.

The development of stresses in growing oxides may result in scale lift-off followed by the development of porosity. If lift-off is followed by scale fracture, then the newly exposed metal will exhibit very rapid oxidation.

Electrical conductivity of oxides

Oxide growth can be compared with a current flow around a circuit containing an electrolytic cell. Oxide growth is characterized by the ionization of metal and oxygen atoms. These are anodic and cathodic processes, respectively. While the metal ions, or cations, are attracted toward the anodic surface, the oxygen ions, or anions, are attracted to the cathodic surface. During oxide growth there may be migration of both cations and anions, or only one species may migrate while the other remains immobile.

While oxidation occurs by ionic transport, there must be electron movement toward the cathode. This movement is largely determined by the activity gradient, in accordance with Fick's laws. It is expected that hanging carbon steel coupons in this research will exhibit mechanisms similar to those outlined above.

Galvanic corrosion

A metal or alloy has a unique corrosion potential, E_{corr}, when immersed in an electrolyte. When two dissimilar metals are coupled in an electrolyte, a galvanic cell is created. In this cell, the metal or alloy with the more negative E_{corr} is active, while the other

metal or alloy is passive (noble) with respect to the active metal or alloy. The active component of the galvanic couple has an excess of electrons that are lost to the noble component. In the galvanic cell, the anodic corrosion reaction is given as

$$M \rightarrow M^{+} + ne^{-} \qquad (2\text{-}1)$$

whose rate is increased by the loss of electrons. The noble metal in the galvanic cell undergoes the corrosion reaction given by

$$N \rightarrow N^{+} + me^{-} \qquad (2\text{-}2)$$

which is decreased due to the presence of electrons drawn from metal M.

Figure 2.1 shows the galvanic series for several alloys in sea water. The most active alloy (negative) in the couple is attacked preferentially by galvanic corrosion. The driving force for galvanic corrosion in any galvanic couple is the difference in corrosion potential of the respective components. Hence, a couple consisting of alloys with small potential difference will suffer galvanic corrosion to a lesser degree than a couple having a large potential difference. The galvanic series gives only tendencies for galvanic corrosion and provides no information regarding rates of attack. The galvanic series for sea water does not necessarily predict the behavior of galvanic couples in different environments. A galvanic series can be generated for any number of environmental conditions. The galvanic series for sea water, however, is a good reference due to the high conductivity of sea water.

In aqueous solutions, the primary cathodic reaction is the reduction of dissolved oxygen at the metal surface according to

$$O_2 + 4H^{+} + 4e^{-} \rightarrow 2H_2O \qquad (2\text{-}3)$$

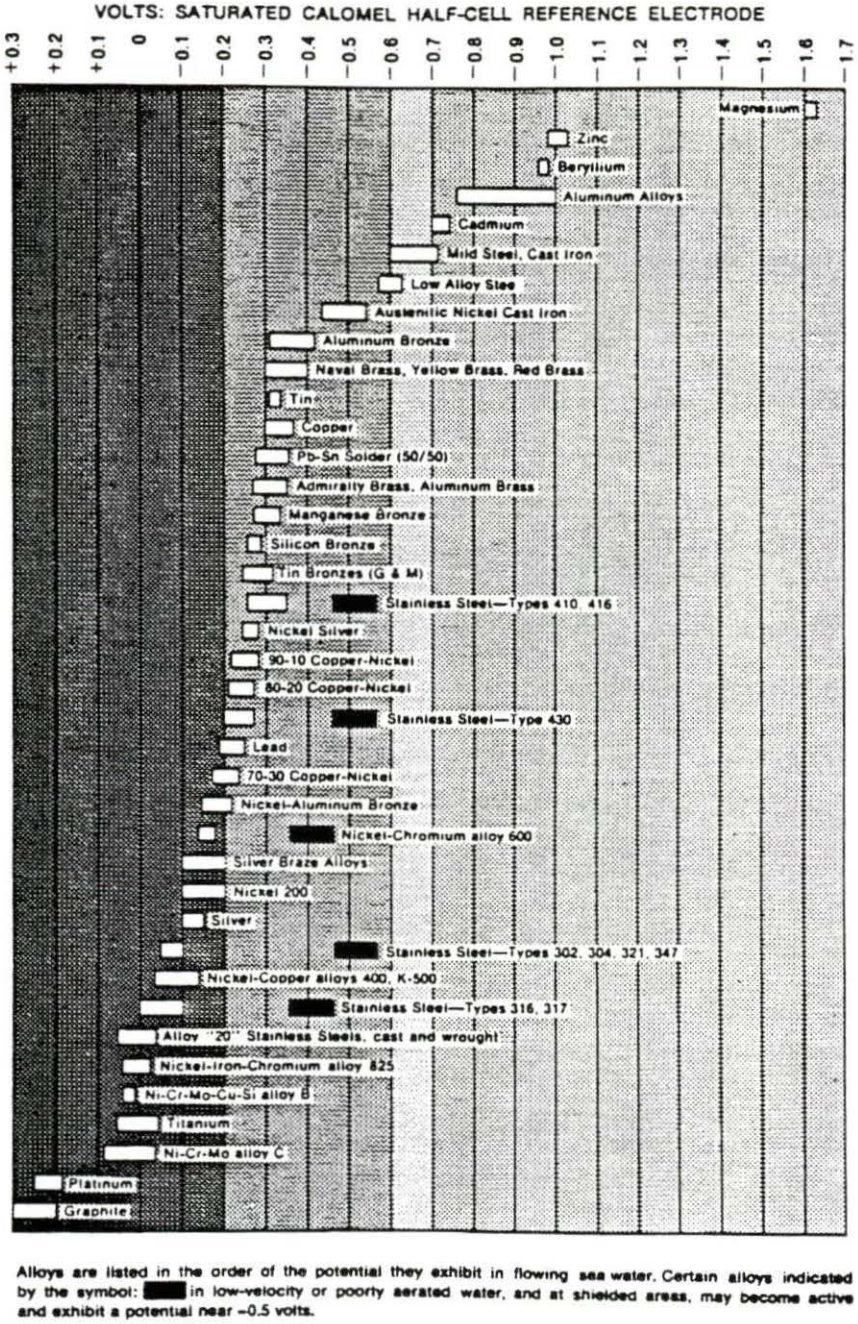

Figure 2.1. Galvanic series for various metals in sea water [8, p.179].

The maximum rate at which dissolved oxygen can be reduced is limited by the rate at which oxygen can diffuse to the cathode surface. Under stagnant conditions, as in this study, the galvanic corrosion rate is under cathodic diffusion control. If the solution is not stagnant, the availability of oxygen is increased, resulting in an increased corrosion rate.

Galvanic corrosion is affected by the surface area of the anode relative to the cathode. A large ratio of cathode/anode surface areas will lead to enhanced corrosion of the anode. Galvanic corrosion is reduced when the cathode/anode ratio is small. Experimental procedures for galvanic corrosion experiments in this research consisted of large cathode/anode ratios.

The rate at which oxygen can be reduced at the cathode also depends on the nature of the film adhering to the surface of the metal or so-called "passive layer." If the cathode surface layer is not present or is unstable in a given environment, the reduction of oxygen occurs and the corrosion rate increases. Galvanic corrosion is reduced when the surface layer on the cathode is stable. In this research, the austenitic alloy, Carpenter 20, is expected to maintain a very stable passive layer. The less noble carbon steel coupons in the galvanic experiments are expected to corrode by mechanisms similar to those described by equation 2-1.

Radiolysis

Dry air systems (mixtures of oxygen and nitrogen) have been more extensively studied than moist air systems. Since there is no water present, the radiation chemistry is relatively simple. The addition of water vapor to the system results in more difficulty in identifying

mechanisms involved. There have been few published studies on the radiation chemistry of air containing appreciable amounts of water. This section presents generally accepted mechanisms involved in irradiated oxygen/nitrogen and oxygen/nitrogen/water environments.

Radiolysis in moist air environments can result in the formation of radiolysis products, including HNO_3, HNO_2, H_2O_2, N_2O_4, NO_2, N_2O, NO, and O_3 [9]. The radiolysis products can result in the production of significant quantities of nitric acid and other oxidizing products with even a limited amount of water vapor and air present. Exposure of water vapor to radiation environments expected at the outer surface of high-level radioactive waste packages could produce significant quantities of HNO_3 and other oxidizing species. A review of selected studies concerned with the radiation chemistry of oxygen/nitrogen/water systems is summarized as follows [9].

The energy absorption for gamma radiation in a moist air environment initially results in the production of the following primary products.

$$N_2 \xrightarrow{\gamma} N_2^+, N^+, N_2^*, N, e^- \qquad (2\text{-}4)$$

$$H_2O \xrightarrow{\gamma} H_2O^+, H_2O^*, H^+, H, OH^+, OH, e^- \qquad (2\text{-}5)$$

$$O_2 \xrightarrow{\gamma} O_2^+, O_2^*, O, O^+, e^- \qquad (2\text{-}6)$$

where the designation "*" signifies an electronically excited state of the species of interest. These radiolysis products combine under various environmental conditions to form a variety of different molecular species.

The oxidation of nitrogen in an irradiation environment has been described by two general mechanisms, ionic and free radical. The ionic mechanism for irradiated oxygen/nitrogen environments, as proposed by Pshezhetsky and Dmitriev [10-12], is described by the following reactions.

$$N_2 \xrightarrow{\gamma} N_2^+ \text{ and } (N_2^+)^* \quad (2\text{-}7)$$

$$N_2^+ + O_2 \rightarrow NO^+ + NO \quad (2\text{-}8)$$

$$(N_2^+)^* + O_2 \rightarrow NO_2^+ + N \quad (2\text{-}9)$$

$$N + O_2 \rightarrow O + NO \quad (2\text{-}10)$$

$$N + O_2 + M \rightarrow O + NO \quad (2\text{-}11)$$

where "M" designates a "third body" molecule signifying that the reaction is termolecular rather than bimolecular.

The free radical mechanism for irradiated oxygen/nitrogen environments was initially proposed by Harteck and Dondes [13-16] and includes the following steps.

$$N_2 \xrightarrow{\gamma} 2N \quad (2\text{-}12)$$

$$O_2 \xrightarrow{\gamma} 2O \quad (2\text{-}13)$$

$$N + O_2 \rightarrow O + NO \quad (2\text{-}14)$$

$$2NO + O_2 \rightarrow 2NO_2 \quad (2\text{-}15)$$

$$N + NO_2 \rightarrow 2NO \quad (2\text{-}16)$$

$$N + NO_2 \rightarrow O + N_2O \quad (2\text{-}17)$$

$$N + NO_2 \rightarrow 2O + N_2 \quad (2\text{-}18)$$

$$N + NO \rightarrow O + N_2 \quad (2\text{-}19)$$

It is difficult to separate ionic, free radical, and excited state processes on a primary reaction level. The identification of these mechanisms becomes even more difficult with the introduction of water vapor. Quantification of the production of nitrates, nitrites, and nitric acid in a moist air radiolysis environment is extremely difficult due to the dynamics of the system and the large number of species produced. Including the aqueous phase of water in the system (as in heterogeneous systems), makes interpretation of the radiation chemistry still more difficult due to the formation of decomposition products of the water.

Related Research

Though the collection of corrosion research is quite volumous, there has been little published work done concerning corrosion in irradiation environments. This section presents the findings of a review of the technical literature relevant to corrosion in irradiated moist air environments.

Nitric acid formation in irradiated moist air environments

Jones [17] was the first to quantify the yield of nitric acid in moist air systems. This study determined the nitric acid yields in irradiated moist air environments up to 1.4 mole percent water vapor using infrared spectroscopy for nitric acid, nitrous oxide, and nitrogen dioxide detection. Findings of Jones' study are summarized herein.

Jones observed that nitric acid and ozone were the major radiolytic products formed initially. In addition, a linear relationship between nitric acid formation and absorbed dose

was noted. Formation of nitric acid was observed to proceed to a total concentration that was stoichiometrically equivalent to the amount of hydrogen initially present in the water. Upon depletion of the water, a decomposition of nitric acid, that was also linear with absorbed dose, was initiated. The nitric acid was found to decompose to water and form a stoichiometrically equivalent amount of nitrogen dioxide. Subsequent to the conversion of nitric acid to nitrogen dioxide, the formation of nitrogen dioxide was observed to continue at a lower rate. Jones found that the ozone initially generated disappeared immediately prior to the depletion of water vapor. Further, it was found that systems initially containing either nitrogen dioxide or a combination of nitrogen dioxide and water resulted in no formation of nitric acid.

Recent work by Tokunaga and Suzuki [18] on the radiolytic removal of NO_2 and SO_2 from flue gases lead to more detailed information on the mechanism for the formation of nitric acid in moist air systems. Researchers irradiated premixed gases composed on nitric acid, air, and water in a flowing system at a temperature of 120 °C. A chemiluminescence type analyzer was used to quantify NO and NO_2 formation. Initially, irradiation was found to decrease the NO concentration, and rapid formation of nitrogen dioxide was observed. The concentration of nitrogen dioxide peaked at a total absorbed dose of 3 Mrad. The decrease in its rate of formation was observed to accompany the initiation of nitric acid formation. In contrast to findings by Jones, nitric acid formation was determined to be a function of the moisture content. Investigators observed no nitric acid formation in dry air and air/nitrogen oxide systems.

Tokunaga and Suzuki proposed the following reaction step for the formation of nitric acid to explain the dependence of nitric acid formation on water content.

$$NO_2 + OH \rightarrow HNO_3 \qquad (2\text{-}20)$$

The presence of water vapor affects the radiation chemistry of the oxygen/nitrogen system in two ways. First, increased moisture content reduces the amount of energy absorbed by the nitrogen, resulting in the formation of atomic nitrogen. This is the key step in the oxidation of nitrogen. Second, based upon reaction (2-20), a necessary step in the oxidation of nitrogen dioxide to form nitric acid is reaction with OH radicals that are generated from the radiolytically induced decomposition of water. It should be noted that the role of water in the formation of nitric acid has not been clearly established.

Work carried out by Wright, et al [19] suggests that, in heterogeneous nitrogen/water and air/water systems, nitric acid production occurs primarily in the vapor phase. Researchers reported a dependency of nitric acid yield on the initial mole fraction of oxygen. The nitric acid yield for air was determined to be 1.5 molecules per 100 eV absorbed by the nitrogen component in the gas phase. This agrees with the value of 1.9 molecules per 100 eV recommended by Burns, et al [20] for the formation of nitric acid in heterogeneous air/water systems.

Metallic corrosion in irradiated moist air environments

Primak and Fuchs [21] investigated the reaction products formed on nickel wire exposed to air systems in the presence of a high mixed gamma/neutron flux. Nickel wire was irradiated in four different gas compositions for varying lengths of time. Investigators

observed no metal nitrates on the nickel surface in experiments that initially contained dry air in the absence of water. Experiments containing only 20 - 30 torr of water and no air resulted in no corrosion products on the nickel wire. Experiments containing a mixture of air and 4 torr water vapor resulted in an increase in the amount of corrosion product on the nickel wire. The observed increase in corrosion product formation was initially linear with exposure time eventually leveling off after 20 MWh of exposure. Experiments containing air initially containing 28 torr of water vapor behaved similarly for early times but remained linear with exposure time up to 50 MWh. Experimental results indicated that both water and air were necessary to the formation of the nitric acid that corroded the nickel wire. In samples containing moist air, the formation of nitric acid was observed to continue until all of the water vapor was depleted from the gas phase. Investigators observed that corrosion ceased once the formation of nitric acid stopped.

Results of recent unpublished work completed by Patterson [22] indicate that the corrosion rates of a low carbon steel and a stainless steel increased with increasing gamma dose rates. The researcher placed carbon steel and stainless steel coupons in Carpenter 20 reaction vessels. These steel coupons were either placed on Ordinary Portland Cement disks or were suspended in the reaction vessel. Methods for introduction of water vapor into the system employed by Patterson were different than those employed in the concrete-buffered experiments of this research, however, results of the concrete-buffered experiments of this research are expected to yield similar results.

The results observed in these two studies indicate that the presence of an irradiation field in a moist air environment leads to enhanced corrosion of nickel wire and carbon steel and stainless steel, respectively. Since current dry storage and deep geologic disposal technologies employ low alloy steels exposed to the atmosphere in the presence of an irradiation field, it is important to quantify the effects of the radiolysis on the corrosion of the storage containers. The work by Primak and Fuchs and by Patterson represents the only known research investigating materials degradation under dry cask storage conditions that has been completed. The present research has been completed to increase the knowledge base concerning the effects of radiolysis products on the corrosion of carbon steel. This research investigates the effects of increasing dose rate on the general and galvanic corrosion of carbon steel in a moist air environment. Further, the present research explores the possible benefits of the introduction of Ordinary Portland Cement into the system.

CHAPTER 3. MATERIALS

Carbon steel coupons used in this experiment were cut from $1/16^{th}$ - inch - thick plate stock obtained from the Engineering Research Institute (ERI) machine shop at Iowa State University (ISU). Coupon dimensions were approximately two centimeters by two centimeters (actual surface areas are reported in the tables of Appendix B). The composition of the carbon steel coupons, as reported by the ERI machine shop, are 0.15 - 0.20 percent carbon, 0.60 - 0.90 percent manganese, 0.04 maximum percent phosphorus, and 0.05 maximum percent sulfur. The carbon steel coupons were exposed in Series 4760 reaction vessels procured from PARR Instrument Company in Moline, Illinois.

The reaction vessels are 300 ml in volume with an inner diameter of 6.35 inches and a depth of 10.01 inches. They were constructed of Carpenter 20 Alloy (35Fe-35Ni-20Cr-2.5Mo-2.0Mn-3.5Cu-1.0Cb max). This austenitic alloy was chosen for its corrosion resistance. The reaction vessels were sealed using a deformable metal gasket consisting of 0.05 millimeter diameter aluminum wire. The aluminum wire was cut into a section with a length slightly larger than the circumference of the reaction vessel. The aluminum section was then shaped into a ring with the ends of the wire overlapped once to minimize leakage. The ring - shaped aluminum wire was placed on the lip of the reaction vessel, where it was anchored using aluminum foil and masking tape. With the gasket in place, the lid of the reaction vessel was placed onto the vessel base and secured with the cap screws. The pressure applied by the cap screws was sufficient to deform the aluminum wire into an

effective gasket. Upon completion of each experiment, the gasket was discarded, and a new gasket was prepared for subsequent experiments.

In order to determine the buffering effect of concrete on the corrosion of the carbon steel coupons, some experiments utilized concrete disks composed of Ordinary Portland Cement (OPC) with fine aggregate. These OPC disks were obtained from the Civil Engineering Department at ISU. The disks are 2 inches in diameter and approximately 0.5 inches thick.

Glass tubing was bent into a "U" shape and placed upside - down in the reaction vessel for some experiments. From the glass tubing, stainless steel spring wire was hung to support carbon steel coupons for subsequent exposure. Several glass Petri dishes were obtained from Chemical Stores at ISU. These dishes were used in the comparison experiments as described in Chapter 4.

Mass measurements were made using an electronic Mettler AE 163 Precision Balance, manufactured by Mettler Instrument Corporation, Hightstown, New Jersey. The balance gives measurements to 10^{-5} grams. During this research, the balance was leveled and calibrated before taking measurements for any single test sample, i.e. before beginning the cleaning procedure on a particular sample and then again before cleaning the next sample.

Sample irradiations were carried out using an underground ^{60}Co source located in the Nuclear Engineering Laboratory at ISU. ^{60}Co is a pure gamma emitter with gamma ray energies of 1.33 and 1.17 Mev. The source consists of several cobalt rods arranged in a circle. Loaded reaction vessels are remotely lowered into the center of the rods. Dose rates

are varied by adjusting the radius of the circular configuration of rods. Low dose rate experiments for this research were carried out with the largest possible radius, while the high dose experiments were carried out with the smallest possible radius.

Since the free energy of formation of the oxide layer on the carbon steel coupons is negative, the surface of a polished carbon steel coupon tends to oxidize quickly when exposed to the atmosphere. In order to limit the oxide formation on the steel surface, a glass dessicator was obtained from Chemistry Stores at ISU for short term storage of the polished carbon steel coupons. The dessicator was filled with an absorbing material to minimize the moisture content of the air in the dessicator.

CHAPTER 4. EXPERIMENTAL PROCEDURES

Preparations

Prior to exposure, each carbon steel coupon was polished to a 600 grit surface, to remove any millscale. The coupon was then dried and weighed four times, using the Mettler balance described in Chapter 3 (the balance was leveled and calibrated prior to measuring a different sample). The average of four weightings for each sample was taken as an unbiased estimate of the true weight of that samples. Once weighed, the samples were immediately placed into the dessicator for not more than 12 hours prior to exposure to their respective test conditions. In all experimental conditions, the dose rate is assumed constant over the duration of the individual exposures and equal to the dose rate at the time of experiment initiation. Also, it is assumed that the gamma rays are unattenuated by the thicknesses of the reaction vessel and of any glassware used in the experiment. This research consisted of three exposure conditions tested under four different experimental conditions. The exposure conditions included tests for the buffering effects of OPC on carbon steel corrosion, tests for the effects of dose rate on galvanic corrosion, and tests for the effects of dose rate on the corrosion of carbon steel in a heterogeneous oxygen/nitrogen/water system (comparison experiments). The four experimental conditions included concrete-buffered experiments, galvanic corrosion experiments, comparison experiments, and combined corrosion experiments, where both galvanic and comparison corrosion conditions were tested.

Concrete-buffered experiments

Concrete-buffered experiments were carried out by placing an OPC disk in the bottom of the reaction vessel. One or two carbon steel coupons were placed, stamped side down, on the OPC disk. Five milliliters (ml) of tap water was added to the concrete disk, which quickly absorbed the water.

These experiments included hanging carbon steel coupons. Once the coupons were in place, the reaction vessel was sealed, and the experiment commenced. The concrete-buffered experiments consisted of exposure to three different dose rates. These dose rates are the control case (10 μrads/hr - background radiation), a low dose rate case, and a high dose rate case. Specifics of each experiment are as follows.

Control -- The control experiment consisted of one hanging sample (BCH) and one lying sample (BCL) exposed to 10 μrads/hr. The exposure began on 10/28/94 at 16:15 hrs and continued uninterrupted until 12/05/94 at 22:35 hrs.

Low dose rate -- The low dose rate experiment consisted of one hanging sample (BLH) and two lying samples (BLL1 and BLL2) exposed to a dose rate of approximately 6643 rads/hr. The irradiation period began on 12/15/94 at 08:29 hrs and continued uninterrupted until 01/19/95 at 09:41 hrs.

High dose rate -- The high dose rate experiment consisted of one hanging sample (BHH) and one lying sample (BHL) exposed to a dose rate of approximately 30414.6 rads/hr. The irradiation period began on 10/28/94 at 16:00 hrs and continued uninterrupted until 12/09/94 at 13:32 hrs.

Galvanic corrosion experiments

Galvanic experiments were carried out by placing a single carbon steel coupon in the bottom of the reaction vessel. Three milliliters of tap water was then added to the reaction vessel around the carbon steel coupon using a pipet to ensure that the top surface of the carbon steel coupon was not wetted. The contact area for each galvanic corrosion experiment is given in Tables B.2 and B.4.

These experiments included carbon steel coupons that were suspended from stainless steel spring wire that was hung on bent glass tubing. Once the coupons were in place, the reaction vessel was sealed, and the experiment commenced. The galvanic corrosion experiments consisted of exposure to two different dose rates. These dose rates are a control case (background radiation) and a high dose rate case. Specifics of each experiments are as follows.

Control -- The control experiment consisted of one hanging sample (GCH) and one lying sample (GCL) exposed to 10 μrads/hr. The exposure began on 03/07/95 at 13:36 hrs and continued uninterrupted until 04/04/95 at 16:18 hrs.

High dose rate -- The high dose rate experiment consisted of two hanging samples (GHH1 and GHH2) and one lying sample (GHL) exposed to a dose rate of approximately 29476.8 rads/hr. The irradiation period began on 01/23/95 at 14:47 hrs and continued until 02/21/95 at 16:24 hrs. This irradiation period was interrupted from 15:20 to 17:10 hrs on 01/31/95, from 07:56 to 20:15 hrs on 02/01/95, from 06:55 to 16:50 hrs on 02/02/95, and from 07:46 to 09:22 on 02/03/95. The interruptions are expected to have little effect on the

corrosion experiments, and exposure duration, given in Table B.2, has accounted for these interruptions.

Comparison experiments

For comparison, a single carbon steel coupon was placed in a Petri dish in the bottom of a reaction vessel for subsequent exposure. Three milliliters of tap water was added to the dish around the lying carbon steel coupon using a pipet to ensure that the top surface of the carbon steel coupon was not wetted.

These experiments also included hanging carbon steel coupons. Once the samples were in place, the reaction vessel was sealed and the experiment commenced. The comparison experiments consisted of exposure to a single dose rate. This dose rate is the control case (background radiation). Specifics of this experiment are as follows.

Control -- The control experiment consisted of one hanging sample (CCH) and one lying sample (CCL) exposed to 10 μrads/hr. The exposure began on 04/05/95 at 12:18 hrs and continued uninterrupted until 05/03/95 at 16:15 hrs.

Combined experiments

Combined experiments, including galvanic corrosion samples and comparison corrosion samples, were carried out by first placing a single carbon steel coupon in the bottom of the reaction vessel. Three milliliters of tap water was then added to the reaction vessel around the carbon steel coupon using a pipet to ensure that the top surface of the carbon steel coupon was not wetted. Next, a 100 ml beaker was placed up - side - down in the reaction vessel. A Petri dish was then placed on top of the beaker. A single carbon steel coupon was

placed in the Petri dish. Three milliliters of tap water was added to the dish around the lying carbon steel coupon using a pipet to ensure that the top surface of the carbon steel coupon was not wetted.

These experiments did not include hanging carbon steel coupons. Once the samples were in place, the reaction vessel was sealed and the experiment commenced. The combined experiments consisted of exposure to three different dose rates. These dose rates are a control case (background radiation), a low dose rate case, and a high dose rate case. Specifics of each experiment are as follows.

Control -- The control experiment consisted of one lying sample exposed to galvanic corrosion conditions (CGCL) and one lying sample exposed to comparison corrosion conditions (CCCL). The dose rate for this experiment was 10 μrads/hr. The exposure began on 05/12/95 at 09:56 hrs and continued uninterrupted until 06/08/95 at 15:45 hrs.

Low dose rate -- The low dose rate experiment consisted of one lying sample exposed to galvanic corrosion conditions (CGLL) and one lying sample exposed to comparison corrosion conditions (CCLL). The dose rate for this experiment was approximately 6382.8 rads/hr. The irradiation period began on 04/05/95 at 11:00 hrs and continued uninterrupted until 05/03/95 at 16:22 hrs.

High dose rate -- The high dose rate experiment consisted of one lying sample exposed to galvanic corrosion conditions (CGHL) and one lying sample exposed to comparison corrosion conditions (CCHL). The dose rate for this experiment was approximately 28342.6 rads/hr. The irradiation period began on 05/12/95 at 10:47 hrs and

continued until 06/08/95 at 15:38 hrs. There was a single interruption in the irradiation period of 42 minutes. This interruption is accounted for in Table B.4.

Cleaning Procedures

Immediately upon completion of respective exposures, reaction vessels were opened, and the carbon steel coupons were promptly analyzed. Each sample was weighed four times on the electronic Mettler balance described in Chapter 3 (the balance was leveled and calibrated before each new sample was analyzed). The average of these four measurements was labeled "C0", indicating that this is the weight for the respective sample after exposure and before any cleaning. The corrosion products were then removed as recommended by the *Annual Book of ASTM Standards*, Volume 3.02 [23]. For cleaning carbon steel test specimens, a solution of 1 liter of hydrochloric acid, 20 grams of antimony trioxide, and 50 grams of stannous (tin) chloride is prescribed. This solution was generally prepared prior to beginning the cleaning procedure. The cleaning procedure is summarized herein.

A single carbon steel coupon is immersed in a fresh, continuously-stirred cleaning solution for a standardized length of time. Initially, this time was set at two minutes (sample BHL), but early results indicated that a shorter time would lead to more accurate estimation of the mass of the corrosion product removed from the surface of the coupon. Therefore, the standardized cleaning time was set to 1.5 minutes for the remainder of the carbon steel coupons. Upon removal from the cleaning solution, the sample was rinsed with acetone and with methanol to assure that the sample would dry thoroughly. The sample was then air dried for 2.5 minutes to allow the methanol to completely evaporate. Next, the sample was

weighed four times. The average of these four measurements was assigned the label "C1", indicating the mass after cleaning one. The procedure was then repeated in a fresh cleaning solution, with the average mass values assigned the appropriate label. This procedure was repeated until the mass change between cleanings reached a relatively constant value. The number of cleanings required to reach a constant mass change varied from 5 to 9 cleanings depending on how well the corrosion product layer adhered to the metal surface.

Calculations

The total mass of the corrosion product formed during the exposure period was obtained by generating a plot of cumulative corrosion mass loss versus cleaning number (see Appendix A). The cumulative corrosion mass loss for the i^{th} cleaning was determined by subtracting the value for the mass after cleaning "i" (Ci, where "i" is the cleaning number) from the mass after exposure but before any cleaning, C0.

Ideally, a plot of cumulative corrosion mass loss versus cleaning number would show a sharp rise in the first few cleanings, and for later cleanings, the cumulative corrosion mass loss would be constant (i.e. zero slope). This would indicate a removal of corrosion product from the carbon steel coupon in the first few cleanings, after which, further cleaning would not result in any mass loss, since the corrosion products has been completely removed. However, cleaning solutions that are effective in removing corrosion products will also remove some base metal if the cleaning process is continued. Therefore, we expect that "Corrosion mass loss versus cleaning number" plots will exhibit an initial rise followed by a leveling off and approaching of a small, finite slope. The slope that is approached represents the rate at which

base metal is being dissolved in the cleaning solution. This is the behavior observed in most of the "Corrosion mass loss versus cleaning number" plots encountered in this research.

Once a "Corrosion mass loss versus cleaning number" plot was generated, the data points on the plot were divided into three groups. The first group consisted of the data points from the first few cleanings, representing the removal of corrosion product only. The second group consisted of data points from intermediate cleanings, representing the removal of both corrosion product and base metal. The third group consisted of the data points from the later cleanings, representing the removal of base metal alone.

A least squares linear regression model with the intercept set equal to zero was fitted to the first group of data points. This regression results in a line of the form

$$f_1(x) = b_{11}x, \tag{4-1}$$

where b_{11} is the slope of the first regression line. This equation may be written in matrix form as

$$\underset{n\times 1}{\hat{\mathrm{Y}}_1} = \underset{n\times 1}{\mathrm{X}_1}\ \underset{1\times 1}{\mathrm{b}_1}, \tag{4-2}$$

where n is the number of data points in the regression, because

$$\begin{bmatrix} \hat{\mathrm{Y}}_{11} \\ \hat{\mathrm{Y}}_{12} \\ \hat{\mathrm{Y}}_{13} \\ \vdots \\ \hat{\mathrm{Y}}_{1n} \end{bmatrix} = \begin{bmatrix} x_{11} \\ x_{12} \\ x_{13} \\ \vdots \\ x_{1n} \end{bmatrix} \begin{bmatrix} b_{11} \end{bmatrix} = \begin{bmatrix} b_{11}x_{11} \\ b_{11}x_{12} \\ b_{11}x_{13} \\ \vdots \\ b_{11}x_{1n} \end{bmatrix}. \tag{4-3}$$

b_{11} is calculated by the solving the equation,

$$\underset{1\times 1}{\mathrm{b}_1} = \left[b_{11}\right] = \left(\underset{1\times 1}{\mathrm{X}_1'}\,\underset{1\times 1}{\mathrm{X}_1}\right)^{-1} \underset{1\times 1}{\mathrm{X}_1'}\,\underset{1\times 1}{\hat{\mathrm{Y}}_1}, \tag{4-4}$$

where the prime indicates the transpose of the matrix. This value was inserted into equation (4-1), giving the equation for a line that represents removal of corrosion product only.

A simple least squares linear regression model was fitted to the third group of data points. This regression results in a line of the form

$$f_2(x) = b_{20} + b_{21}x, \tag{4-5}$$

where b_{20} is the y-intercept of the second regression line and b_{21} is the slope. This equation may be written in matrix form as

$$\underset{n\times 1}{\hat{\mathrm{Y}}_2} = \underset{n\times 2}{\mathrm{X}_2}\,\underset{2\times 1}{\mathrm{b}_2}, \tag{4-6}$$

where n is the number of data points in the regression, because

$$\begin{bmatrix} \hat{\mathrm{Y}}_{21} \\ \hat{\mathrm{Y}}_{22} \\ \hat{\mathrm{Y}}_{23} \\ \vdots \\ \hat{\mathrm{Y}}_{2n} \end{bmatrix} = \begin{bmatrix} 1 & x_{21} \\ 1 & x_{22} \\ 1 & x_{23} \\ \vdots & \vdots \\ 1 & x_{2n} \end{bmatrix} \begin{bmatrix} b_{20} \\ b_{21} \end{bmatrix} = \begin{bmatrix} b_{20} + b_{21}x_{21} \\ b_{20} + b_{21}x_{22} \\ b_{20} + b_{21}x_{23} \\ \vdots \\ b_{20} + b_{21}x_{2n} \end{bmatrix}. \tag{4-7}$$

b_{20} and b_{21} was calculated by the solving the equation,

$$\underset{2\times 1}{\mathrm{b}_2} = \begin{bmatrix} b_{20} \\ b_{21} \end{bmatrix} = \left(\underset{2\times 2}{\mathrm{X}_2'}\,\underset{2\times 2}{\mathrm{X}_2}\right)^{-1} \underset{2\times 1}{\mathrm{X}_2'}\,\underset{2\times 1}{\hat{\mathrm{Y}}_2}. \tag{4-8}$$

The calculated values for b_{20} and b_{21} were inserted into equation (4-5), giving the equation for a line that represents removal of base metal only. Determining equations for removal of corrosion product only and for removal of base metal only allows an estimation for the loss of mass of corrosion product by solving the equation,

$$f_1(x_h) = f_2(x_h), \tag{4-9}$$

where x_h represents the x-value at the point where the two lines meet. The y-value of the intersection of these lines, given by $f_1(x_h)$ in equation (4-1), represents an estimate of the mass loss of corrosion product given in the tables of Appendix B as "Corrosion Mass Loss". The second group of data points were not used in the determination of the total mass loss of corrosion product.

Once an estimate for mass loss of corrosion product was determined, the final mass of the sample (included in the tables of Appendix B) was calculated by

Final Mass ≡ (mass @ cleaning 0) - (Corrosion Mass Loss) = C0 - $f_1(x_h)$. (4-10)

The total mass loss of base metal due to corrosion was then calculated by

Total Mass Loss ≡ (Initial Mass) - (Final Mass). (4-11)

The dimensions of each sample was measured, and the total surface area of the respective sample was determined in square decimeters. These values (listed in the tables of Appendix B) were calculated by the following equations.

Hanging samples

$$\text{Surface Area} \equiv 2*l*w + 2*t*(l + w) + \pi*d*t - \frac{\pi * d^2}{2}, \text{ and} \tag{4-12}$$

Contact samples

$$\text{Surface Area} \equiv 2*l*w + 2* t *(l + w), \tag{4-13}$$

where l, w, and t are the length, width, and thickness, of the coupon, respectively, and d is the diameter of the hole used for hanging samples. These surface areas were calculated through the implementation of the FORTRAN program listed in Appendix C.

The exposure duration for each coupon in days was recorded for each sample. The corrosion rate was then calculated by

$$\text{Corrosion Rate} \equiv \frac{1000 * (\text{Total Mass Loss})}{(\text{Surface Area}) * (\text{Exposure Duration})}, \qquad (4\text{-}14)$$

where the units of "Total Mass Loss" is in milligrams, the units of "Surface Area" is in square decimeters, and the units of "Exposure Duration" is in days. Therefore, the units of corrosion rates are milligrams per square decimeter per day (mdd), and these values are reported in the tables of Appendix B.

Error Analysis

In calculating the corrosion rates of carbon steel coupons in a moist air environment subjected to a gamma radiation field, it is necessary to quantify the error associated with the experimental procedures. The largest fraction of experimental error associated with the determination of the corrosion rates occurs in the estimation of the mass loss of corrosion product. This component of the experimental error was calculated by the following procedure.

It is assumed that the mass measurements on the electronic Mettler balance, described in Chapter 3, are independent random observations from a population for which the sample mean is approximately normally distributed. Further, it is assumed that the error associated with the measurements are random, uncorrelated, and unbiased. The latter statement means

that the error associated with the least squares regression accounts for the random variations in the mass values after a given cleaning.

It is expected that the most conservative approach to determining the error associated with the estimation of the corrosion mass loss is to construct prediction intervals for the second linear regression. This is due to the small slope of the second regression line. Since the second regression line is close to horizontal, changes in the first regression line will have relatively little effect on the *y*-value of the intersection of the two lines. Therefore, the error associated with a prediction of the value for corrosion mass loss at the intersection of the two regression lines, with 95 percent certainty, is given by

$$error = \pm t_{(.025,n-2)} * \mathrm{MSE} * (1 + X_h' (X_2' X_2)^{-1} X_h), \tag{4-15}$$

where $t_{(.025;n-2)}$ is the test statistic for the 95th percentile of the *t* distribution with (*n*-2) degrees of freedom,

$$\mathrm{MSE} \equiv \frac{Y_2' Y_2 - b_2' X_2' Y_2}{n-2},$$

and

$$X_h \equiv \begin{bmatrix} 1 \\ x_h \end{bmatrix}.$$

The errors associated with an unbiased estimate of the initial mass and the post-exposure mass, C0, are determined by

$$error = \pm s * (1.96), \tag{4-16}$$

where s is the estimated standard deviation of the sampling distribution of the specific mass measurement. The factor, 1.96, represents the 95th percentile of the standard normal distribution.

Other sources of experimental error are in the determination of the exposure duration and the surface area of the carbon steel coupon. Experiment initiation times and experiment conclusion times are expected to be accurate to within 15 minutes per handling occurrence (i.e., an uninterrupted corrosion experiment would be assigned an error of ± 30 minutes). For the purpose of surface area calculation, the FORTRAN program listed in Appendix C was implemented. This program assumes that each distance measurement has an error of ± 1 %, and the errors are propagated by the following rules.

Given: $u = x + y$ *or* $u = x - y$

$$\sigma_u = (\sigma_x^2 + \sigma_y^2)^{1/2} \tag{4-17}$$

Given: $u = x * y$ *or* $u = x / y$

$$\sigma_u = u*((\sigma_x / x)^2 + (\sigma_y / y)^2)^{1/2}, \tag{4-18}$$

where σ represents the error associated with a given experimental value.

As the corrosion rate of a carbon steel sample is calculated by equations (4-10), (4-11) and (4-14), the error is propagated by the appropriate rule as given by equations (4-17) and (4-18). Error analysis data are given in the tables of Appendix D.

CHAPTER 5. RESULTS

Concrete-buffered experiments -- The carbon steel coupons included as the control specimens for the concrete-buffered experiments showed a corrosion rate of 0.12 mdd for the coupon in contact with the concrete and 0.10 mdd for the hanging coupon. An average corrosion rate of 1.57 mdd was observed for the contact samples exposed at the low dose rate, while a corrosion rate of 0.19 mdd was observed for the hanging sample at the same dose rate. The coupons exposed at the high dose rate in the concrete-buffered experiments exhibited corrosion rates of 2.09 mdd and 0.22 mdd for the contact sample and the hanging sample, respectively. These and other data relevant to the concrete-buffered experiments are included in Table B.1 of Appendix B.

Data from the concrete-buffered experiments indicate an increase in corrosion rate with increasing dose rates for both hanging samples and contact samples. A graphical summary of the concrete-buffered experiments is given in Figure 5.1. The data in Figure 5.1 show that the increase in corrosion rate realized by increasing the dose rate from the control dose rate to approximately 6643 rads/hr is much greater than the corrosion rate increase achieved by increasing the dose rate from approximately 6643 rads/hr to approximately 30414.6 rads/hr. Further, the data indicate that contact samples corrode at significantly higher rates than do hanging samples when radiolysis products are introduced. However, the contact sample in the control case exhibited only a slightly greater corrosion rate than the corrosion rate experienced by the hanging sample (0.12 mdd and 0.10 mdd, respectively).

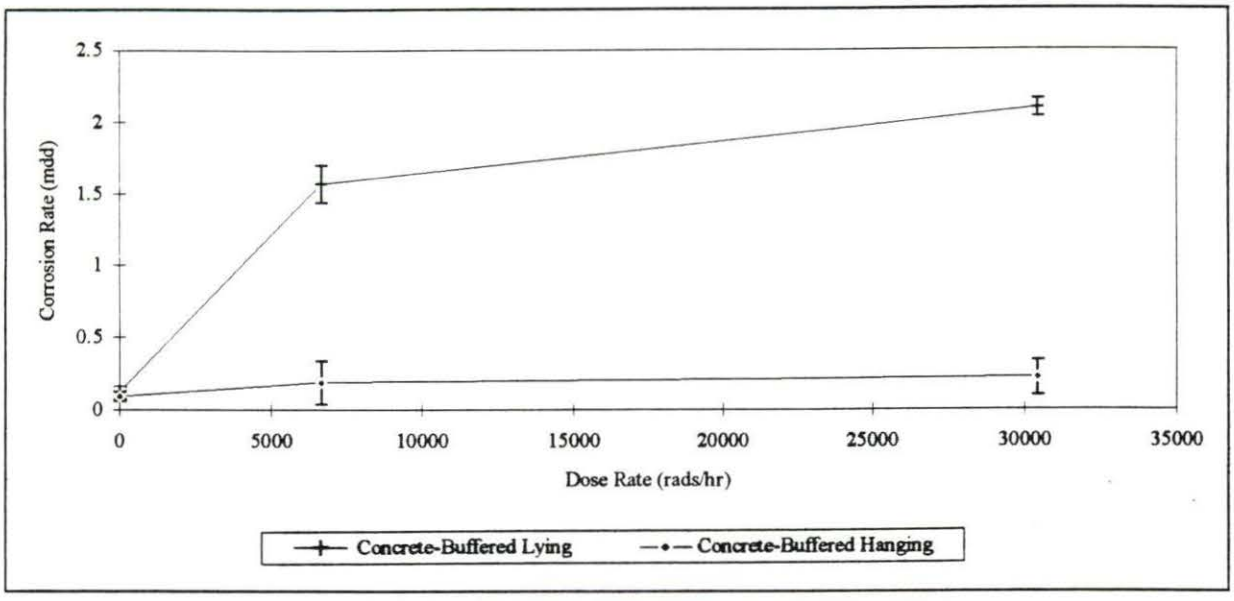

Figure 5.1. Corrosion rate data for concrete-buffered experiments.

Galvanic corrosion experiments -- The carbon steel coupons included as the control specimens for the galvanic experiments showed corrosion rates of 24.97 mdd and 0.42 mdd, respectively, for the contact and hanging coupons. At the high dose rate, a corrosion rate of 35.10 mdd was observed for the contact sample, and an average corrosion rate of 0.18 mdd was observed for the hanging samples. These and other data relevant to the galvanic experiments are included in Table B.2 of Appendix B.

Data from the galvanic corrosion experiments are summarized in Figure 5.2. These data indicate a corrosion rate increase of 10.13 mdd for a carbon steel coupon exposed at approximately 29476.8 rads/hr as compared to the carbon steel coupon exposed in the control case (35.10 mdd and 24.97 mdd for the high dose rate case and control case, respectively). From Figure 5.2, it appears that the corrosion rate for the hanging samples actually decrease

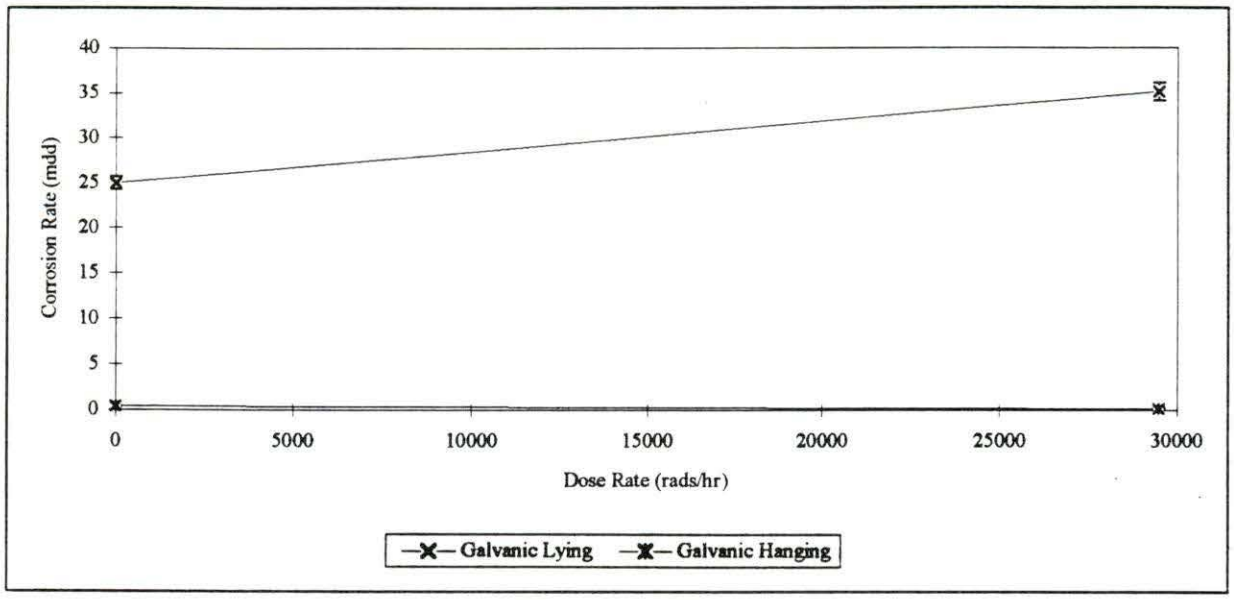

Figure 5.2. Corrosion rate data for galvanic corrosion experiments.

as the dose rate is increased. This seems inconsistent with the data observed for the hanging samples exposed in the concrete-buffered experiments. However, this occurrence may be attributed to the ambient conditions during exposure.

The high dose rate experiment was initiated on 01/23/95, while the control experiment was initiated on 03/07/95. It is expected that the higher mean temperature during control experiment may have resulted in an increased humidity in the reaction vessel. This increased humidity is expected to have increased the corrosion rate of the carbon steel coupon exposed in the control experiment by increasing the amount of water on the surface of the hanging coupon. Alternately, it is expected that corrosion rates of contact samples in all experiments would be affected to a lesser extent than the hanging samples. Corrosion of the lying samples

tended to be concentrated on the bottom surface of the coupon, which remained wet throughout the experimental exposure.

Comparison experiments -- The carbon steel coupons included in the comparison experiments were exposed at the control dose rate only. A corrosion rate of 12.12 mdd was observed for the contact sample, and a corrosion rate of 0.32 mdd was observed for the hanging sample. These and other data relevant to the comparison experiments are included in Table B.3 of Appendix B.

Combined experiments -- The carbon steel coupons included in the control of the combined experiments showed corrosion rates of 22.19 mdd exposed to galvanic corrosion conditions and 14.16 mdd exposed to comparison corrosion conditions. At the low dose rate, the corrosion rates were determined to be 13.12 mdd for the coupon exposed to galvanic corrosion conditions and 9.24 mdd for the coupon exposed to comparison corrosion conditions. Corrosion rates of 30.13 mdd and 10.84 mdd were observed for coupons exposed to galvanic corrosion conditions and comparison corrosion conditions, respectively. These and other data relevant to the combined experiments are included in Table B.4 of Appendix B.

Data from the combined experiments are summarized in Figure 5.3. Figure 5.3 indicates that the samples exposed to the galvanic corrosion conditions corrode at a higher rates than the samples exposed to the comparison corrosion conditions at all dose rates. However, the data suggest that corrosion rates decrease as the dose rate is increased from the control dose rate to approximately 6382.8 rads/hr followed by increased corrosion rates for the carbon steel coupons exposed at approximately 28342.6 rads/hr. The shape of the

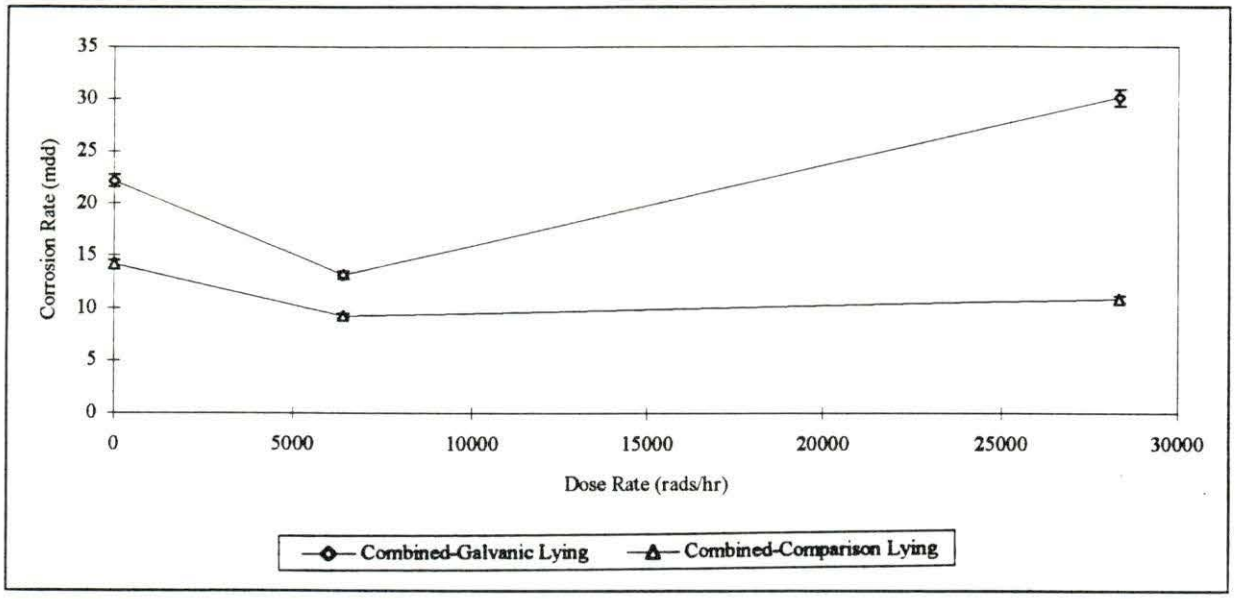

Figure 5.3. Corrosion rate data for combined corrosion experiments.

corrosion rate curve for the combined galvanic corrosion experiments (the upper curve) may be due to the cleaning of the reaction vessels prior to the control and high dose rate experiments.

The galvanic corrosion experiments resulted in the deposition of significant corrosion products from the degradation of the carbon steel coupons on the bottom of the reaction vessels. Having been clean initially, it was considered unnecessary to clean the vessel prior to early galvanic experiments. However, these early galvanic experiments contaminated the vessels for later experiments. Therefore, the vessels were cleaned with a dilute hydrochloric acid solution prior to the control and high dose rate experiments. This cleaning effectively removed the reaction vessel's protective oxide layer that had been present in all prior experiments. Since the presence of an oxide layer inhibits corrosion by mechanisms described

in Chapter 2, the cleaning of the reaction vessels resulted in an upward shift in the corrosion rate curve for the galvanic corrosion experiments at the control and high dose rates.

The validity of the control and high dose rate data is supported by analysis of Figure 5.4. The top corrosion rate curve represents the data obtained in the galvanic corrosion rate experiments and the next lower curve represents the data obtained in the galvanic corrosion

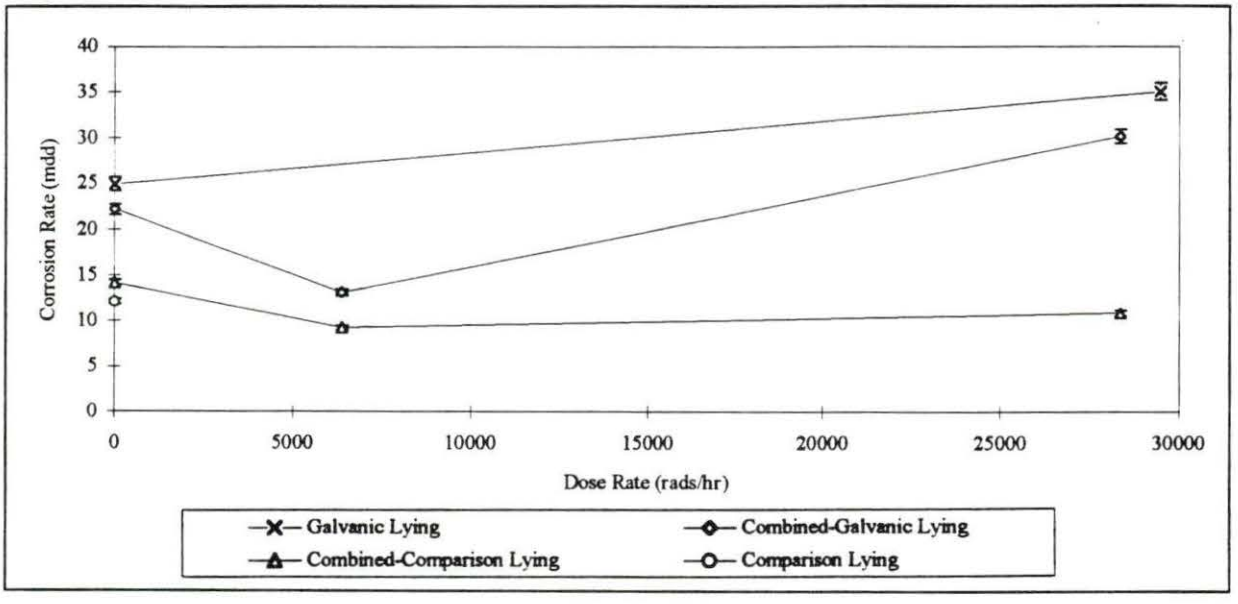

Figure 5.4. Corrosion rate data for galvanic, comparison, and combined corrosion experiments.

rate conditions of the combined experiments. A line extending from the corrosion rate at the control dose rate to the corrosion rate at the high dose rate of the combined-galvanic corrosion experiments (lower curve of Figure 5.4) would result in a line that is nearly parallel to the galvanic corrosion rate curve.

The position of the galvanic corrosion curve in Figure 5.4 (upper curve) relative to the position of the coupons exposed to the galvanic corrosion conditions of the combined corrosion experiments suggest that the increase in corrosion rates due to the cleaning of the reaction vessels is significant. The volume of the reaction vessels used in the galvanic corrosion experiments is 300 ml. The galvanic corrosion conditions of the combined corrosion experiments were characterized by a decreased volume of only 100 ml. Decreased volume results in a decrease in the volume of air available for the formation of radiolysis products. Therefore, corrosion rates for the galvanic corrosion experiments are expected to be significantly higher than corrosion rates for the galvanic corrosion conditions of the combined corrosion experiments due to this volume reduction.

In addition, the introduction of glassware within the reaction vessel in the combined experiments resulted in a significant increase in the surface area inside the container. Since radiolysis products are primarily produced in the vapor phase and are removed from the vapor via adsorption or condensation on surfaces, the relative concentration of detrimental radiolysis products is lower for higher surface areas. This reduction in concentration could lead to a lower corrosion rate.

Data from the comparison corrosion conditions of the combined corrosion experiments indicate a decrease in the corrosion rate as the dose rate is increased from the control dose rate to approximately 6382.8 rads/hr followed by an increase in the corrosion rate as the dose rate is increased from approximately 6382.8 rads/hr to approximately 28342.6 rads/hr (lower curve of Figure 5.3). An explanation for the shape of this curve is unclear.

Further, it is not clear how the cleaning of the reaction vessels would have affected the corrosion rates in these experiments.

CHAPTER 6. CONCLUSIONS

Experimental data indicate that the corrosion rate of carbon steel increases when exposed to gamma radiation, similar to the results found by Patterson. Analysis of the data suggests that this increase in corrosion rate is not linear with increasing dose rate. Rather, the carbon steel exhibits a relatively sharp increase with increased dose rate at lower dose rates followed by a less marked corrosion rate increase at higher dose rates.

A summary of experimental corrosion rate data is given in Figure 5.5. Analysis of this figure indicates that the introduction of OPC to the system may provide a beneficial buffering effect on the corrosion of carbon steel. Carbon steel coupons exposed in the concrete-buffered experiments were found to corrode five times slower than coupons exposed to comparison corrosion conditions when exposed to gamma radiation. Carbon steel coupons exposed to galvanic corrosion conditions showed corrosion rates that were up to three times greater than those exposed to comparison corrosion conditions and up to fifteen times greater than those exposed to concrete-buffered conditions.

The experimental results of this research project may have great implications on technology employed for both high and low level radioactive waste disposal. It is apparent that a carbon steel cask exposed to the atmosphere in a radiation environment will encounter enhanced corrosion of the outer surface of the cask. Also, it is apparent that the presence of OPC may act as a buffer by absorbing some radiolysis products from the vapor surrounding the cask. Although the corrosion rates of the concrete-buffered experiments are relatively low, the increase due to the introduction of a radiation field is significant.

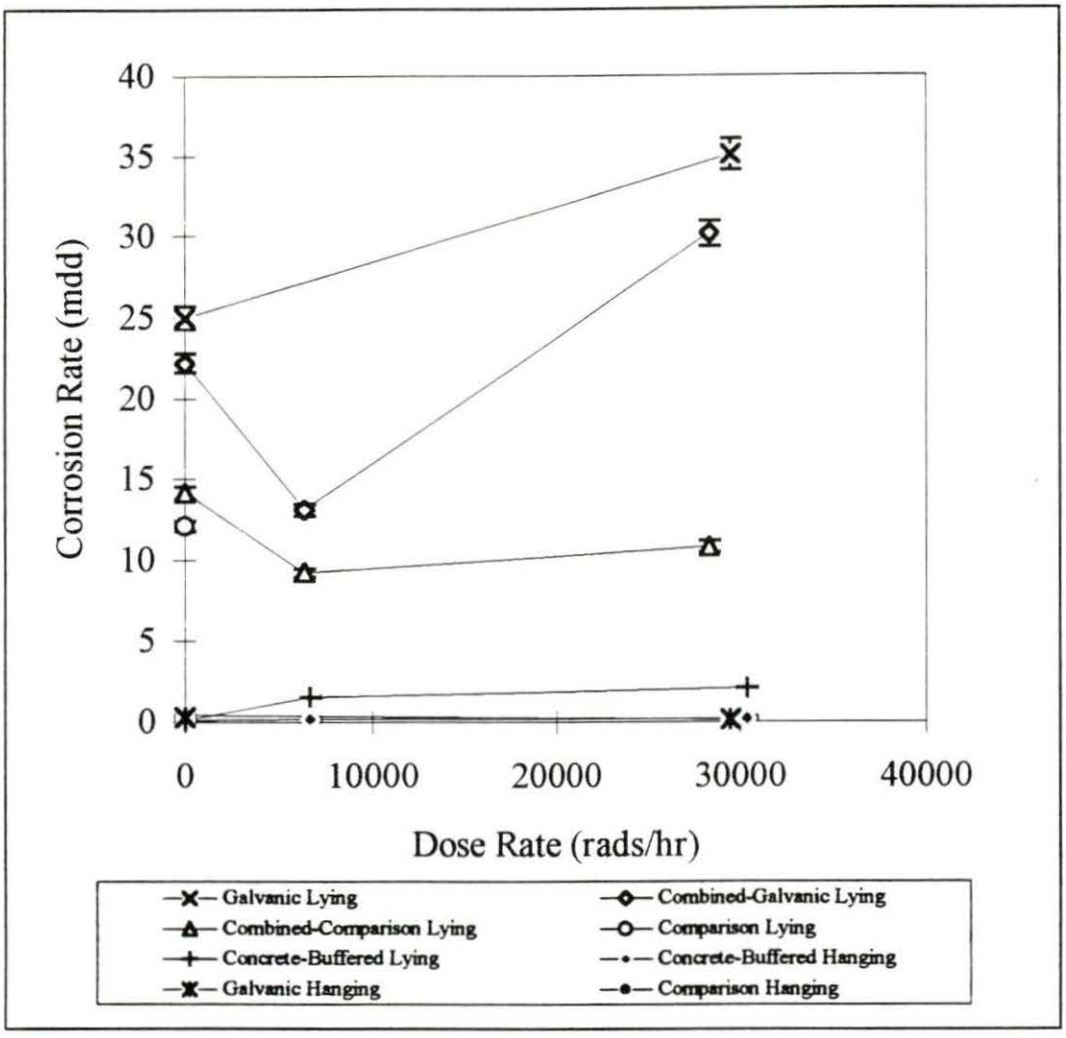

Figure 5.5. Corrosion rate data for all corrosion conditions considered.

Results further suggest that long term performance of storage containers may be affected by the formation of radiolysis products. Upon breaching the outer storage container, or corrosion allowance material, it is likely that a galvanic cell would be formed inside of this container with the container liner, or inner container. The data show that the result of the formation of such a galvanic cell would be a greatly increased corrosion rate (nearly 1500%).

The presence of radiolysis products would further enhance corrosion of the metals involved in the galvanic cell. It is therefore important to maintain the integrity of the corrosion allowance material in order to avoid the formation of a galvanic cell. Therefore, it may be necessary to employ fully self-shielded containers for the disposal radioactive waste. Using fully self-shielded containers would result in the lowest possible rates of degradation of a given corrosion allowance material and lead to the longest container life by eliminating the effects of radiation in forming nitric acid and other oxidizing species.

Data suggest that the ambient environment during exposure may impact the results of corrosion experiments. Therefore, for future corrosion experiments, it is important to control the environment in which the experiments are carried out in order to limit this effect. An alternative suggestion is to expose all experimental units simultaneously and in the same environment.

If industry is driven by economics to dispose of waste in containers other than fully self-shielded containers, further research is necessary to determine the long-term effects of dose rate and temperature on the degradation of candidate container materials in an irradiation environment. Additional research is necessary to determine the corrosion rate at dose rates below the low dose rates studied in this experiment and to determine if there is a threshold dose rate below which there are no significant increases in corrosion rate. Also, it is important to determine the effects of temperature on the corrosion rates of candidate container materials. Since the present research is carried out at ambient temperature, data

may not fully explain the behavior of candidate materials at higher temperatures. Experiments should be completed at temperatures more consistent with the expected service environments.

Further, it is necessary to conduct corrosion experiments in which candidate container materials are exposed for longer periods of time than those analyzed in this research. Long-term exposure data of candidate container materials in environments other than radiation environments are abundant. These data suggest that most metals corrode quickly for a short period of time after initiation of corrosion experiments. The high initial corrosion rates generally decrease to a constant, small, finite corrosion rate as exposure time increases due to the buildup of corrosion products on the surface of the metal. It is expected that metals exposed in a radiation environment would behave similarly, however, no significant research has been conducted to support this assertion. Therefore, it is important to perform corrosion experiments in radiation environments with exposure lasting as long as several years in order to determine if a relatively, steady-state corrosion rate occurs with steels in radiation environments.

REFERENCES CITED

[1] "Nuclear Waste Policy Act of 1982," United States Statutes at Large, Volume 96 part 2, Public Law 97 - 425, January 7, 1983, 96 Statute 2201 - 2261.

[2] "Nuclear Waste Policy Amendment Act of 1982," United States Statutes at Large, Volume 101 part 2, Public Law 100 - 203, December 22, 1987, 101 Statute 1330 - 227 to 1330 - 255.

[3] Tang, Y. S. and Saling, J. H. Radioactive Waste Management; Hemisphere Publishing Corporation: Washington, (1990).

[4] "Spent Nuclear Fuel Discharges from U. S. Reactors 1990," Service Report, Energy Information Administration: SR/CNEAF/92-01, Washington, D. C., (1992).

[5] "Guidebook on Spent Fuel Storage, Second Edition," International Atomic Energy Agency (IAEA): Technical Report Series, Number 240, Vienna, (1991).

[6] Webster's Ninth New Collegiate Dictionary, Merriam - Webster, Inc., Publishers: Springfield, Massachusetts, (1986).

[7] Vinson, D. W., Nutt, W. M., and Bullen, D. B. "Survey of Degradation Modes of Candidate Materials for High - Level Radioactive - Waste Containers: Iron - Base, Corrosion - Allowance Materials," Lawrence Livermore National Laboratory Report UCRL-CR-120464, August 1994.

[8] LaQue, F. L. Marine Corrosion: Causes and Prevention, John Wiley & Sons, New York, (1975) p. 179.

[9] Reed, D. T. and Van Konynenburg, R. A. "Effect of Gamma Radiolysis on Waste Package Components," Scientific Basis for Nuclear Waste Management X, Proceedings of Materials Research Society, Volume, 112, (1988) pp. 393 - 404.

[10] Pshezhetsky, S. V. and Dmitriev, M. T. "Nitrogen Fixation by the Action of Ionizing Radiations," Int. J. Appl. Radiat. Isotop., Volume 5, (1959) p. 67.

[11] Dmitriev, M. T. "The Primary Ions Responsible for the Radiation - Induced Oxidation of Nitrogen," Russ. J. Phys. Chem., Volume 40, (1966) p. 939.

[12] Dmitriev, M. T. "The Role of the Recombinations of Electrons and Ions in the Radiation - Induced Oxidation of Nitrogen," Russ. J. Phys. Chem., Volume 40, (1966) p. 819.

[13] Harteck, P. and Dondes, S. "Radiation Chemistry of Gases," Proc. 2nd Int. Conf. Peaceful Uses of Atomic Energy, United Nations, Geneva, Volume 29, (1958) p. 415.

[14] Harteck, P. and Dondes, S. "Nitrogen Pentoxide Formation by Ionizing Radiation," J. Chem. Phys., Volume 28, (1958) p. 975.

[15] Harteck, P. and Dondes, S. "Decomposition of Nitric Oxide and Nitrogen Dioxide by the Impact of Fission Fragments of Uranium - 235," J. Chem. Phys., Volume 27, (1957) p. 546.

[16] Harteck, P. and Dondes, S. "The Kinetic Equilibrium of Air," J. Phys. Chem., Volume 63, (1959) p. 956.

[17] Jones, A. R. "Radiation - Induced Reactions in the N_2 - O_2 - H_2O System," Rad. Res., Volume 10, (1959) p. 655.

[18] Tokunaga, O. and Suzuki, N. "Radiation Chemical Reactions in NO_x and SO_2 Removals from Flue Gas," Radiat. Phys. Chem., Volume 24, (1984) p. 145.

[19] Wright, J., Linacre, J. K., Marsh, W. R., and Bates, T. H. "Effect of Radiation on Heterogeneous Systems of Air or Nitrogen and Water," Proc. Int. Conf. on the Peaceful Uses of Atomic Energy, Volume 17, (1956) p. 560.

[20] Burns, W. G., Hughes, A. E., Marples, J. A. C., Nelson, R. S., and Stoneham, A. M. "Radiation Effects and the Leach Rates of Vitrified Radioactive Waste," Nature, Volume 295, (1982) p. 130.

[21] Primak, W. and Fuchs, L. H. "Nitrogen Fixation in a Nuclear Reactor," Nucleonics, Volume 13, (1955) p. 38.

[22] Patterson, A. J. M.S. Thesis, Iowa State University, 1994.

[23] Annual Book of ASTM Standards -- Section 3: Metals Test Methods and Analytical Procedures, Volume 3.02: Wear and Erosion; Metal Corrosion, American Society of Testing and Materials, Philadelphia, (1990).

ACKNOWLEDGMENTS

In completing this thesis, I was assisted by a number of people. While it is not possible to name everyone, I would like to acknowledge those people that were most helpful.

First and foremost, I would like to thank Dr. Bullen for his time and technical assistance. Also, thanks for his confidence and guidance throughout my graduate work. For her immeasurable assistance and guidance, I would like to thank Becky Staedtler. It was she who helped make sense of the many deadlines and much of the paperwork required of this graduate student. Without her assistance, these requirements would have been unbearable.

Thanks to the faculty members of the Nuclear Engineering Program at Iowa State University and to the members of my committee for their time and contribution to my work. And thank you to the National Academy for Nuclear Training (INPO) and to Iowa State University for financial support of my graduate degree. Finally, I owe a great deal to my fiancee, Jessica, for her encouragement and tolerance.

APPENDIX A. CORROSION MASS LOSS PLOTS

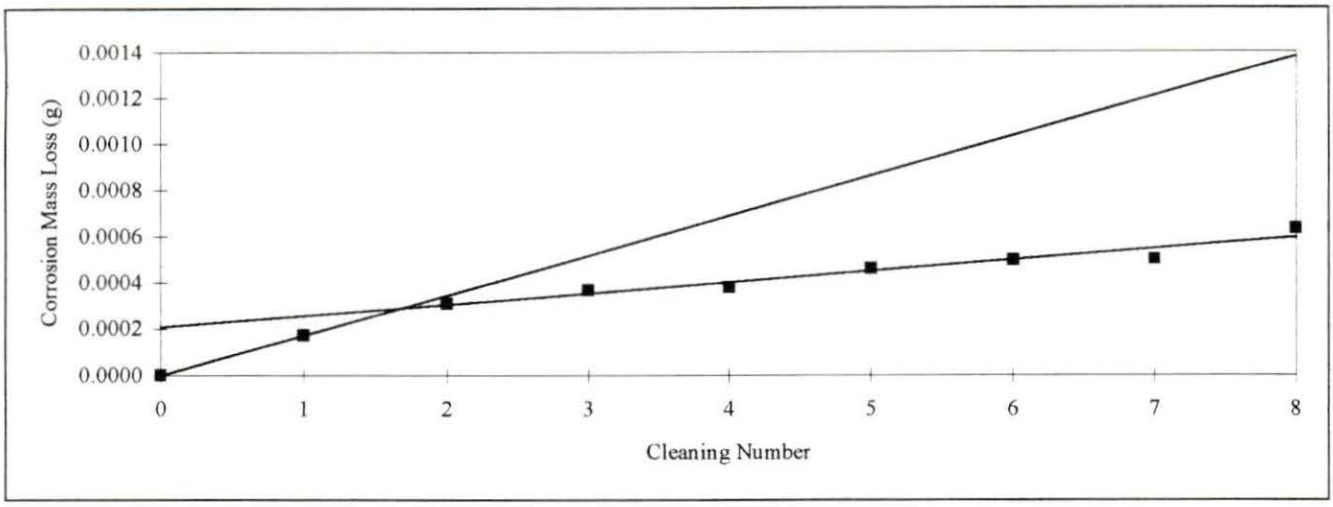

Figure A.1. Corrosion mass loss plot for the hanging sample exposed at the control dose rate in the concrete-buffered experiments.

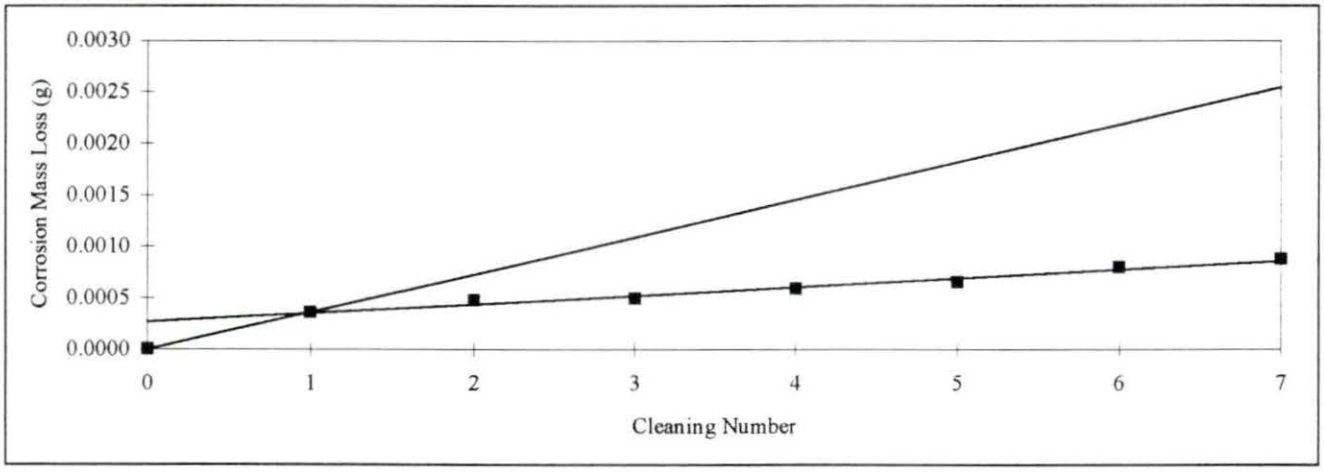

Figure A.2. Corrosion mass loss plot for the lying sample exposed at the control dose rate in the concrete-buffered experiments.

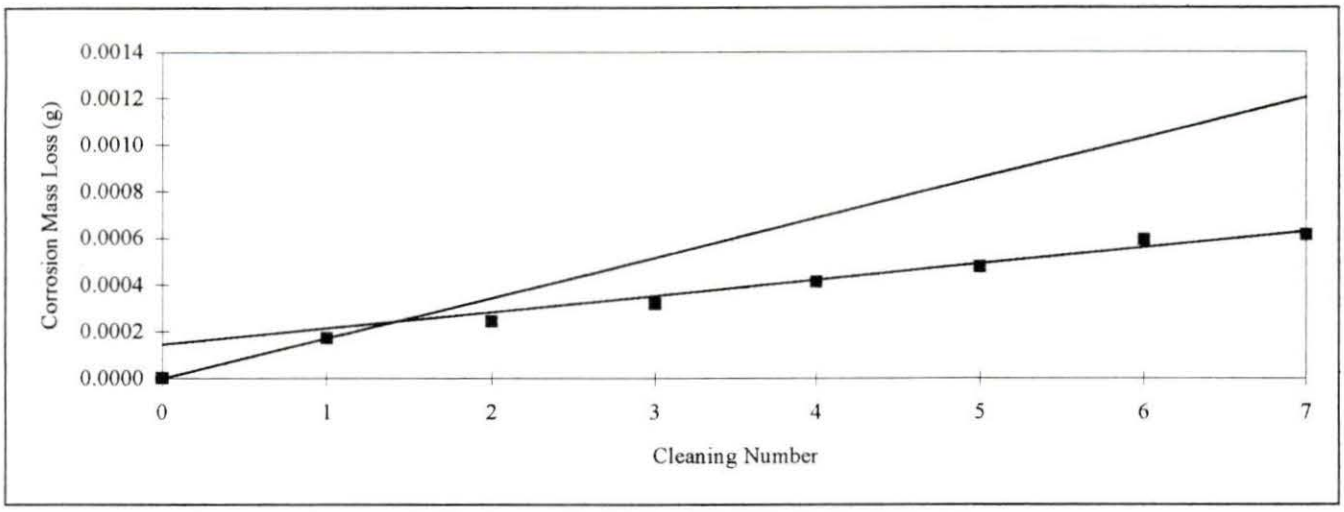

Figure A.3. Corrosion mass loss plot for the hanging sample exposed at the low dose rate in the concrete-buffered experiments.

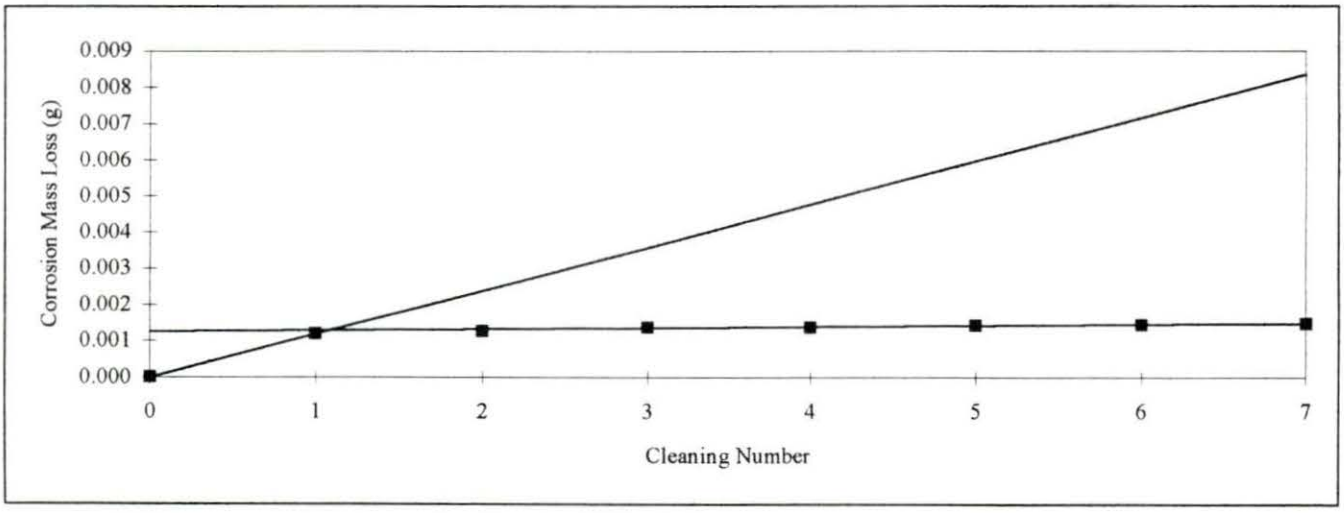

Figure A.4. Corrosion mass loss plot for the first lying sample exposed at the low dose rate in the concrete-buffered experiments.

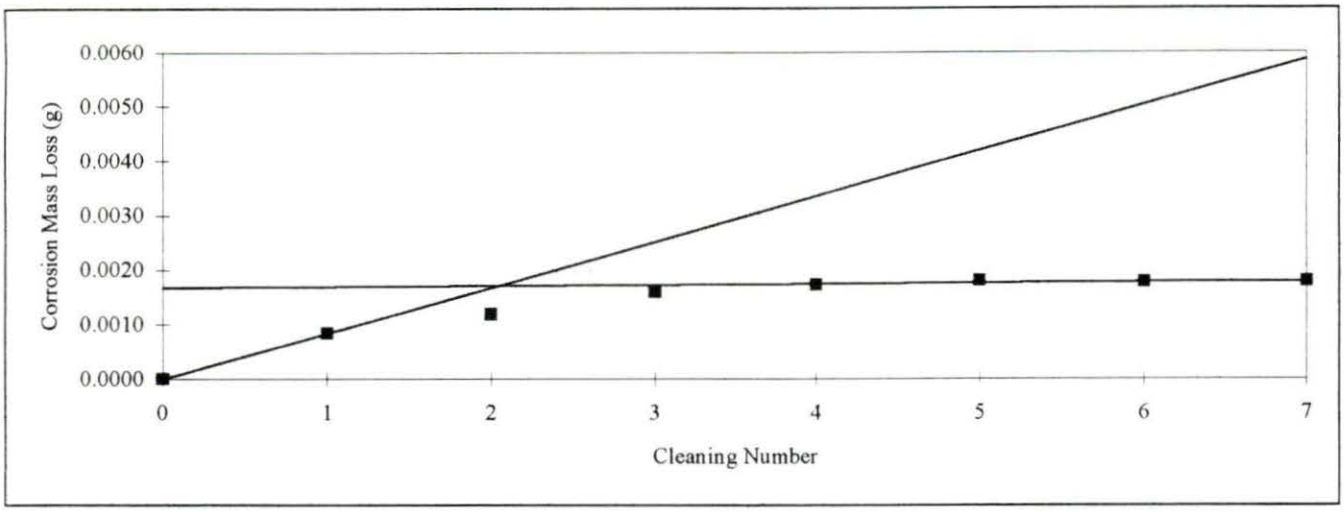

Figure A.5. Corrosion mass loss plot for the second lying sample exposed at the low dose rate in the concrete-buffered experiments.

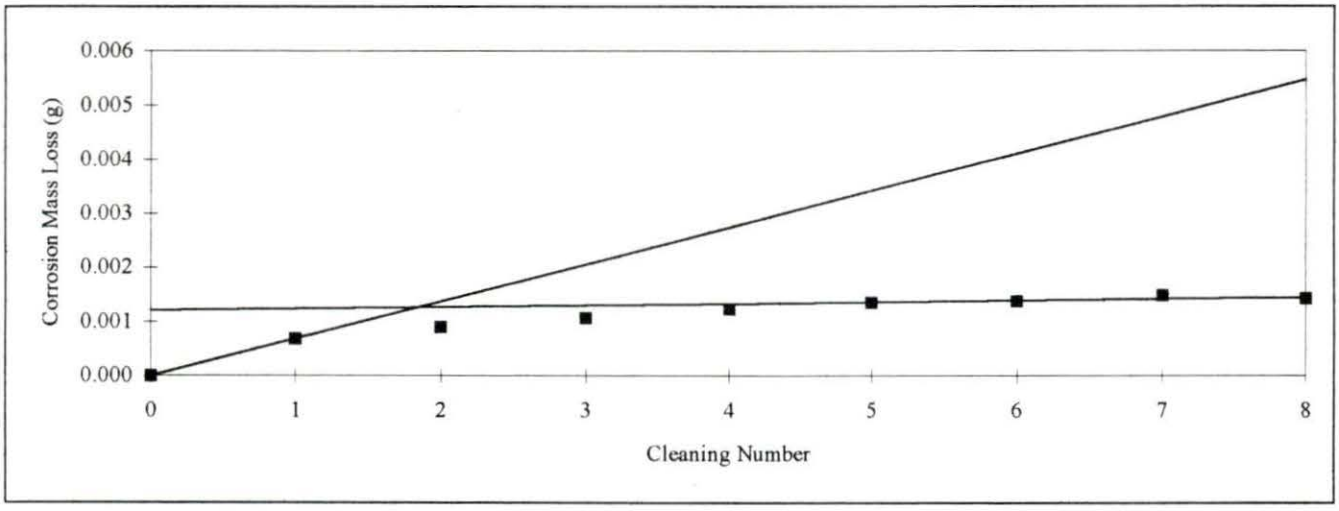

Figure A.6. Corrosion mass loss plot for the hanging sample exposed at the high dose rate in the concrete-buffered experiments.

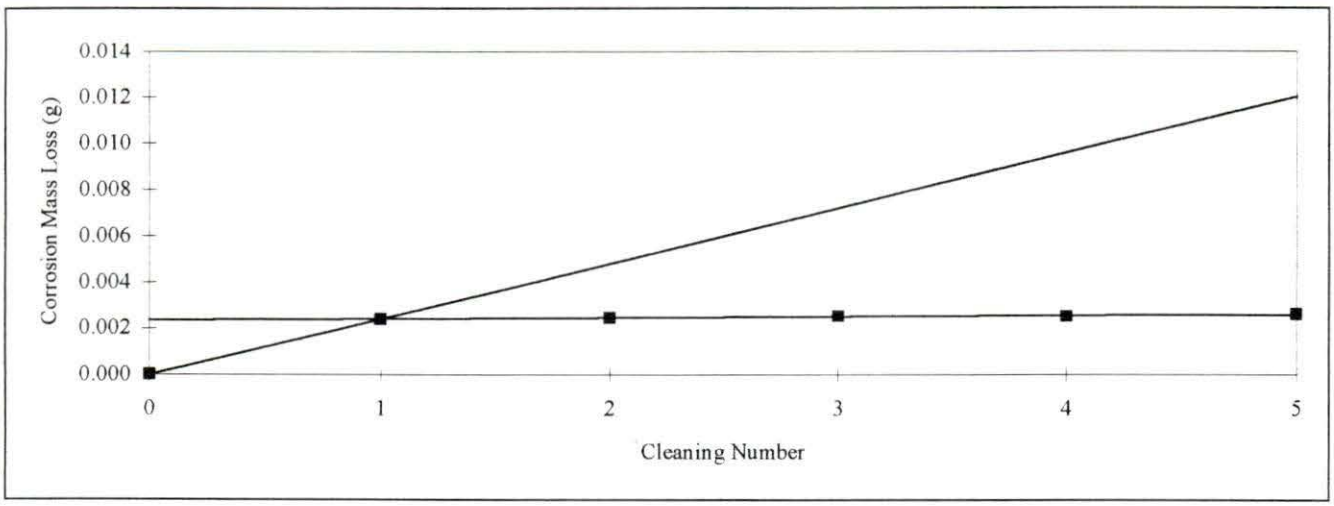

Figure A.7. Corrosion mass loss plot for the lying sample exposed at the high dose rate in the concrete-buffered experiments.

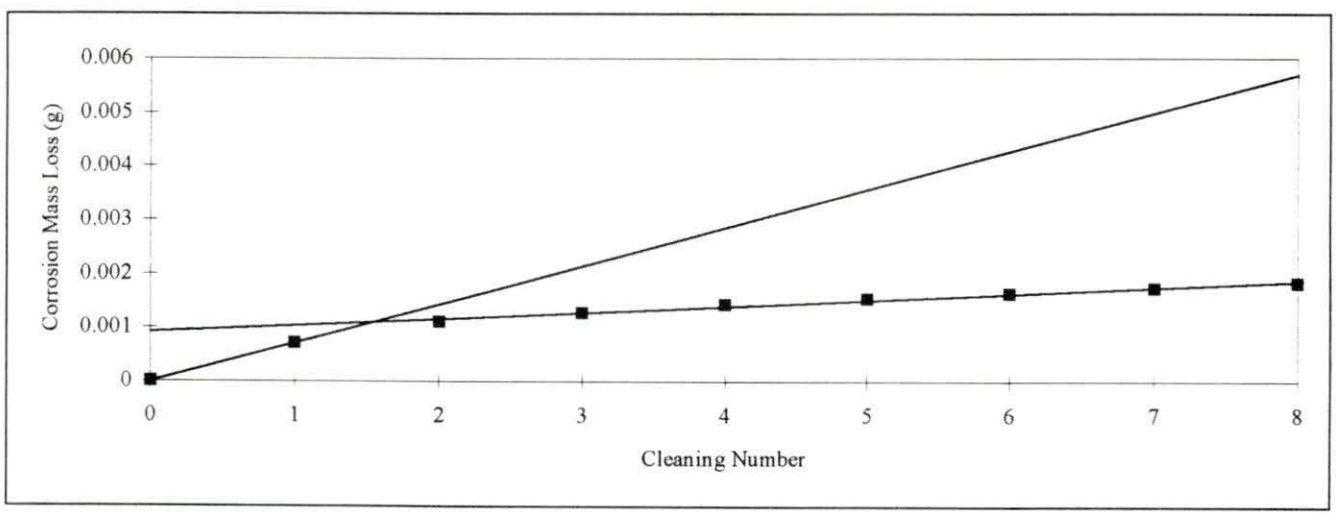

Figure A.8. Corrosion mass loss plot for the hanging sample exposed at the control dose rate in the galvanic experiments.

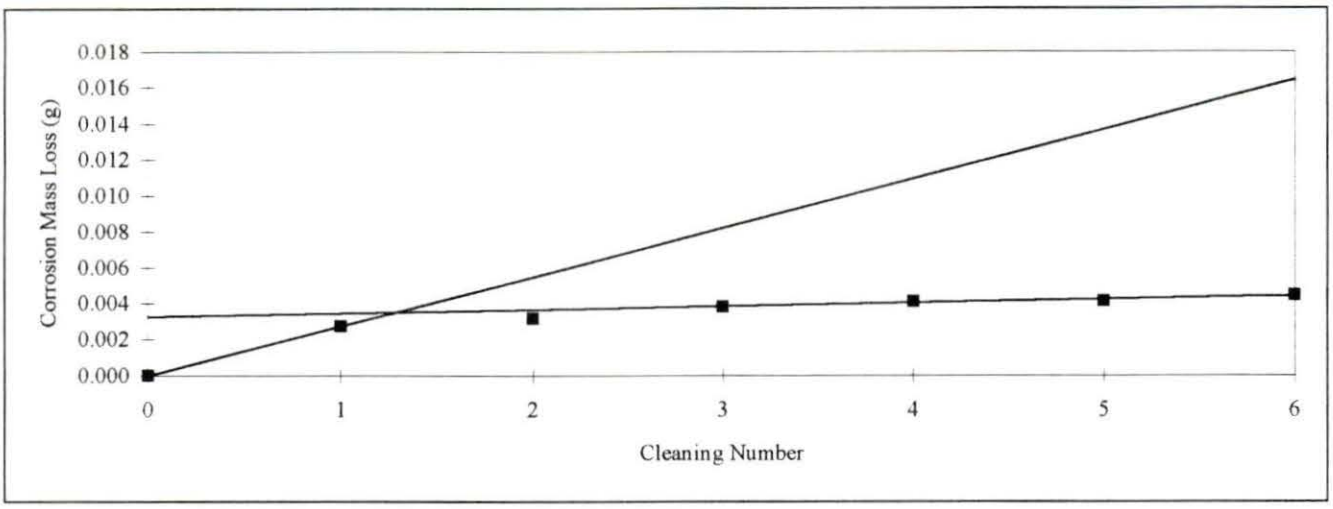

Figure A.9. Corrosion mass loss plot for the lying sample exposed at the control dose rate in the galvanic experiments.

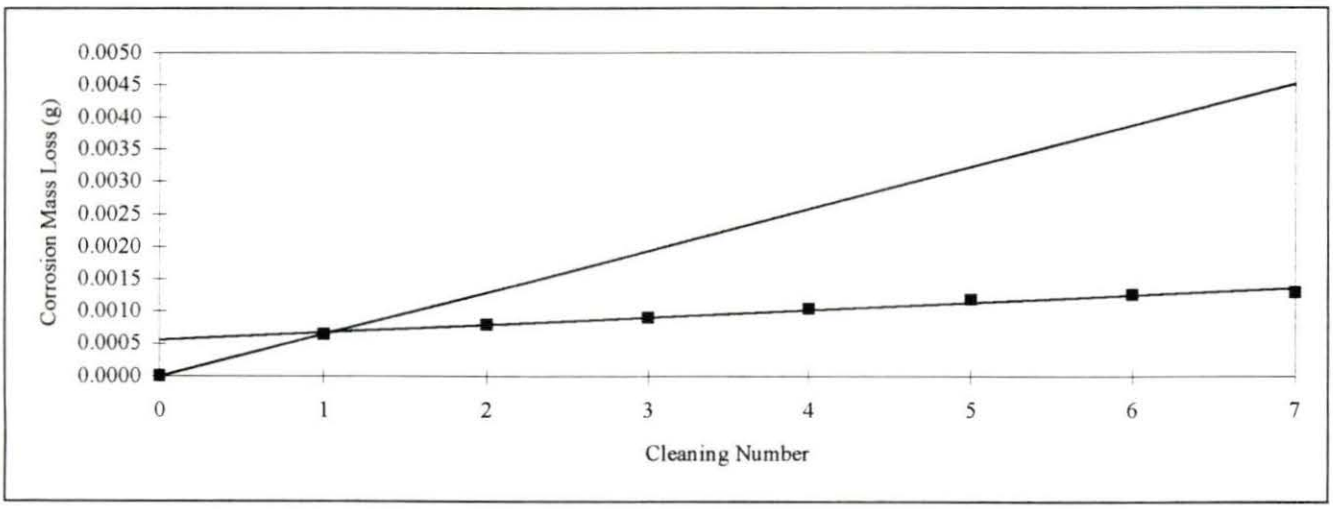

Figure A.10. Corrosion mass loss plot for the first hanging sample exposed at the high dose rate in the galvanic experiments.

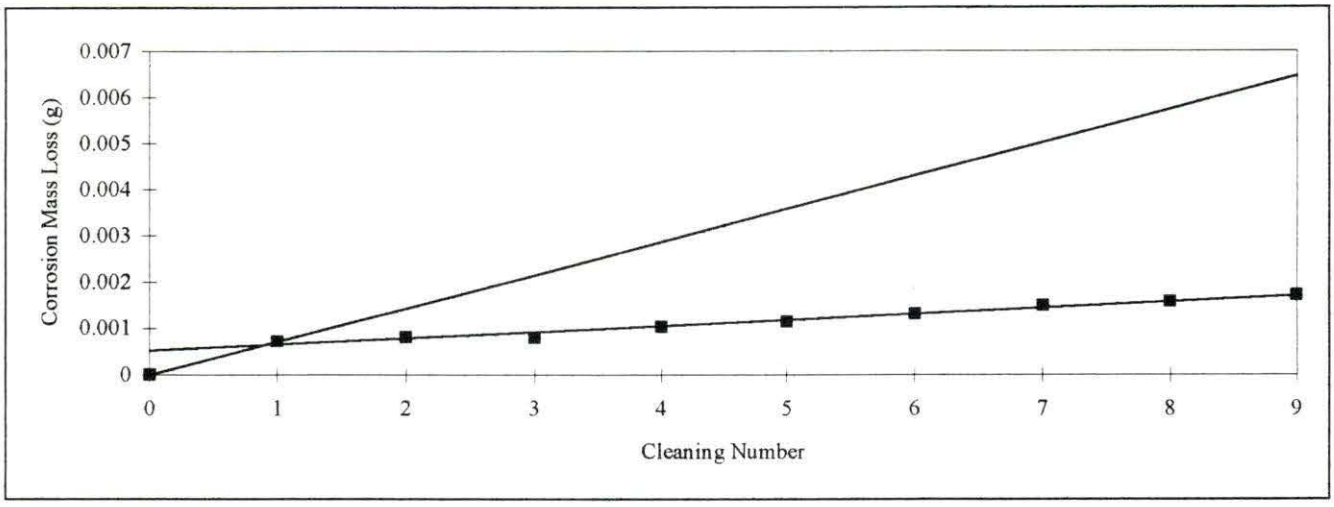

Figure A.11. Corrosion mass plot for the second hanging sample exposed at the high dose rate in the galvanic experiments.

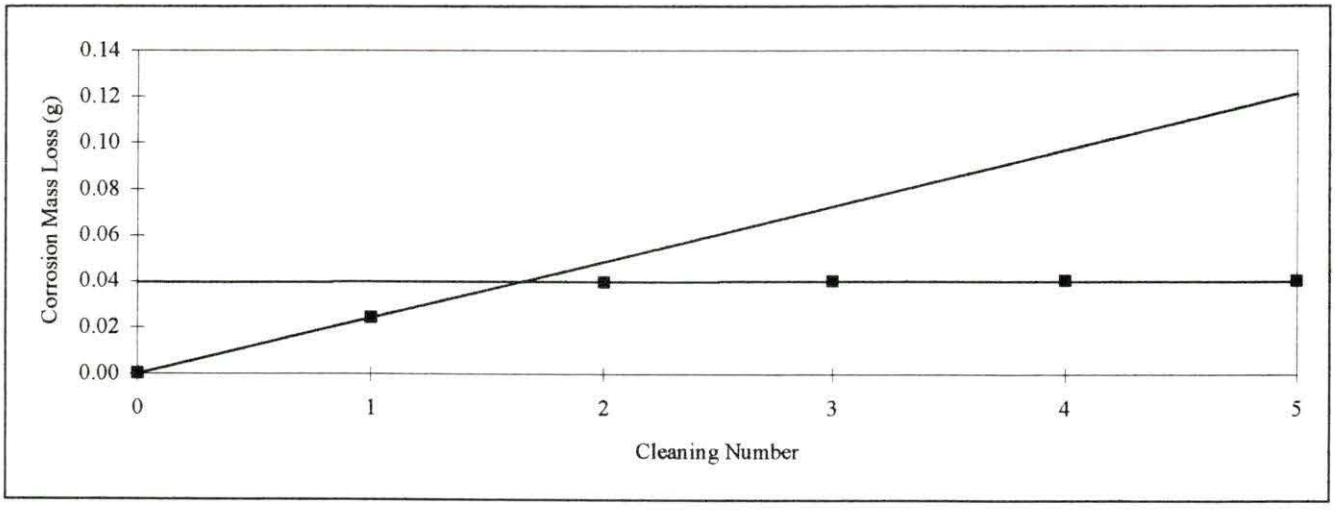

Figure A.12. Corrosion mass plot for the lying sample exposed at the high dose rate in the galvanic experiments.

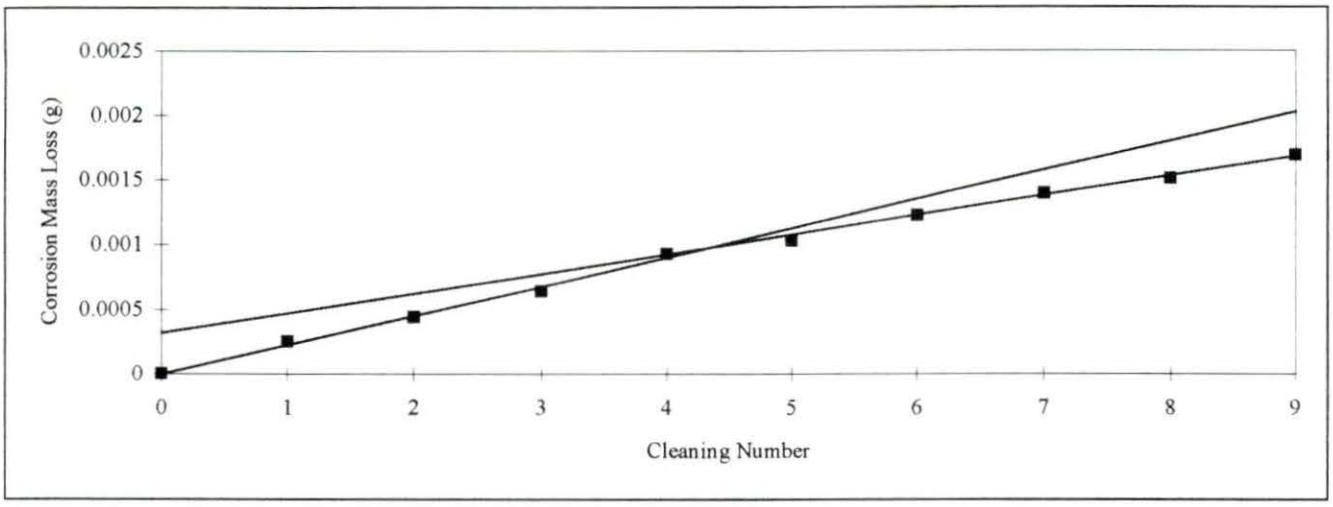

Figure A.13. Corrosion mass loss plot for the hanging sample exposed at the control dose rate in the comparison experiments.

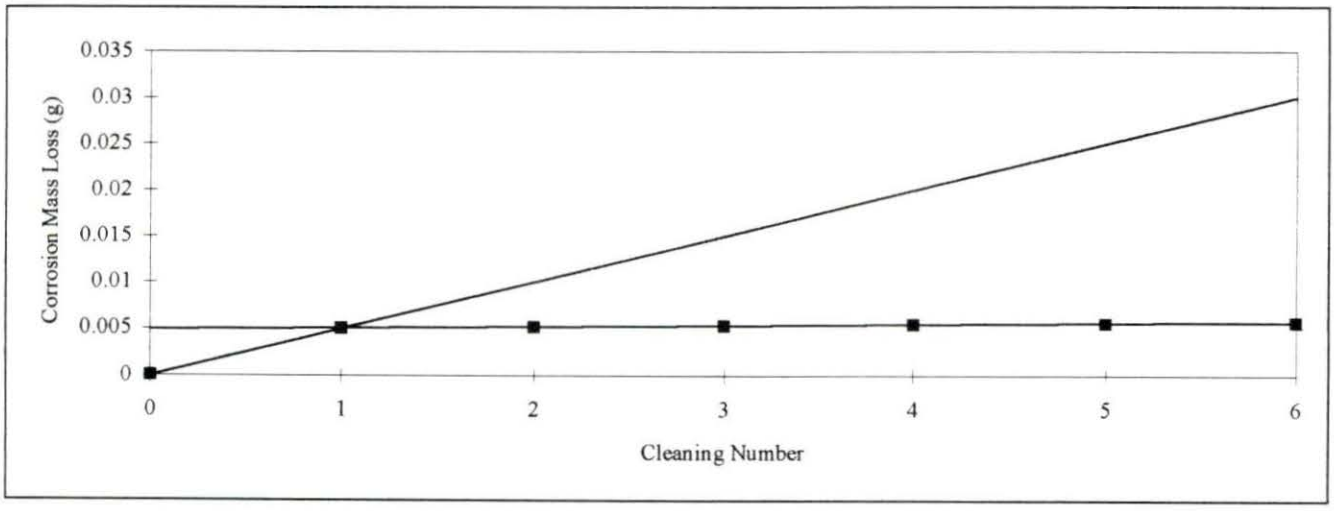

Figure A.14. Corrosion mass loss plot for the lying sample exposed at the control dose rate in the comparison experiments.

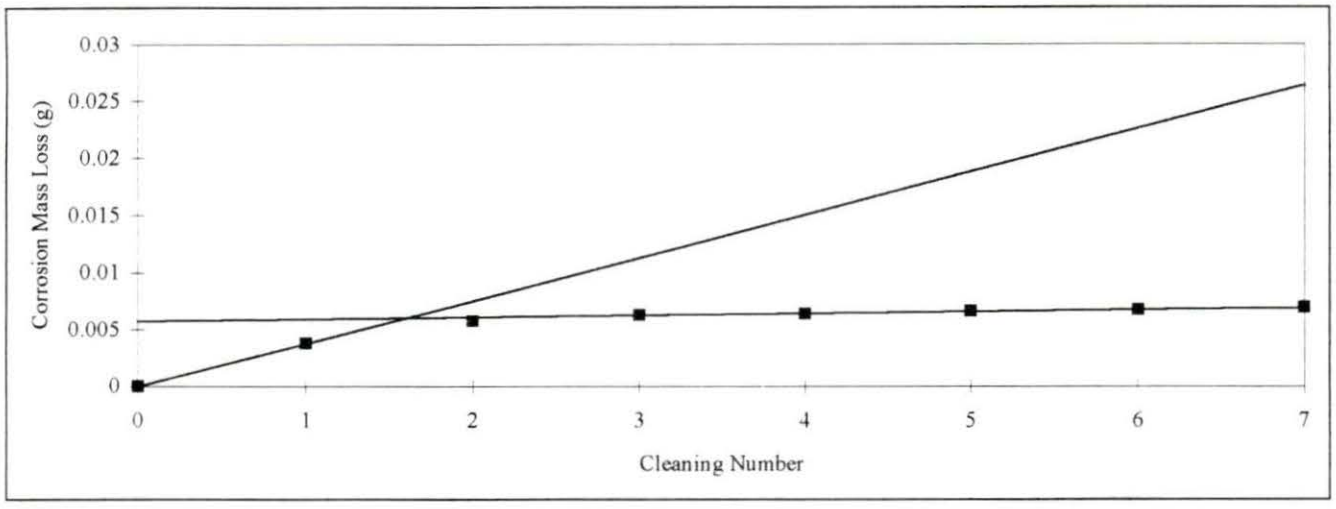

Figure A.15. Corrosion mass plot for the lying sample exposed at the control dose rate under the galvanic conditions of the combined experiments.

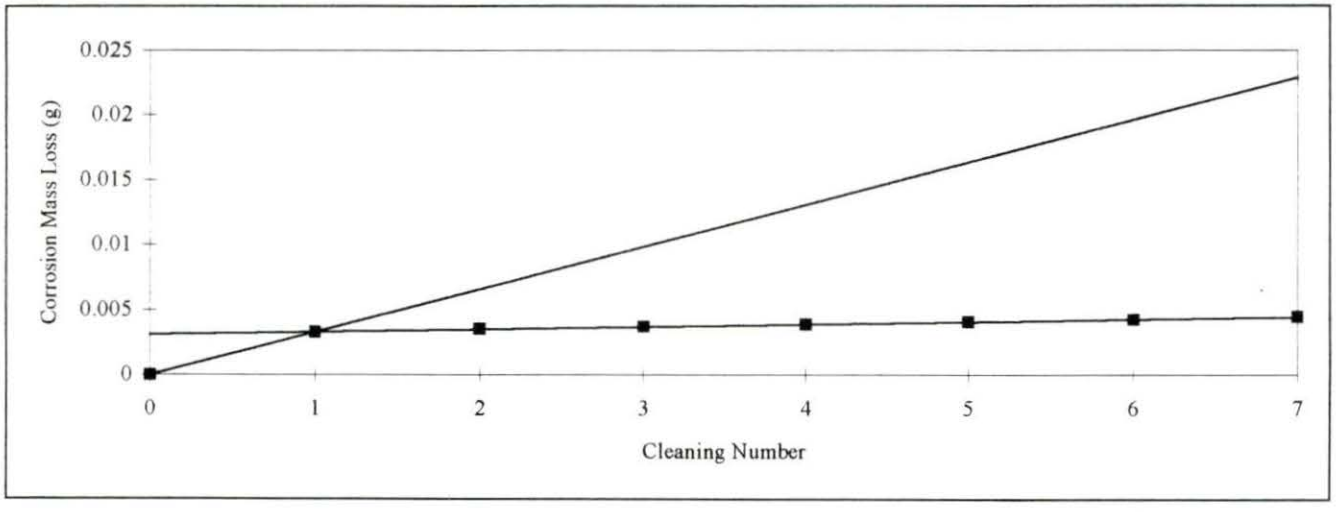

Figure A.16. Corrosion mass plot for the lying sample exposed at the control dose rate under the comparison conditions of the combined experiments.

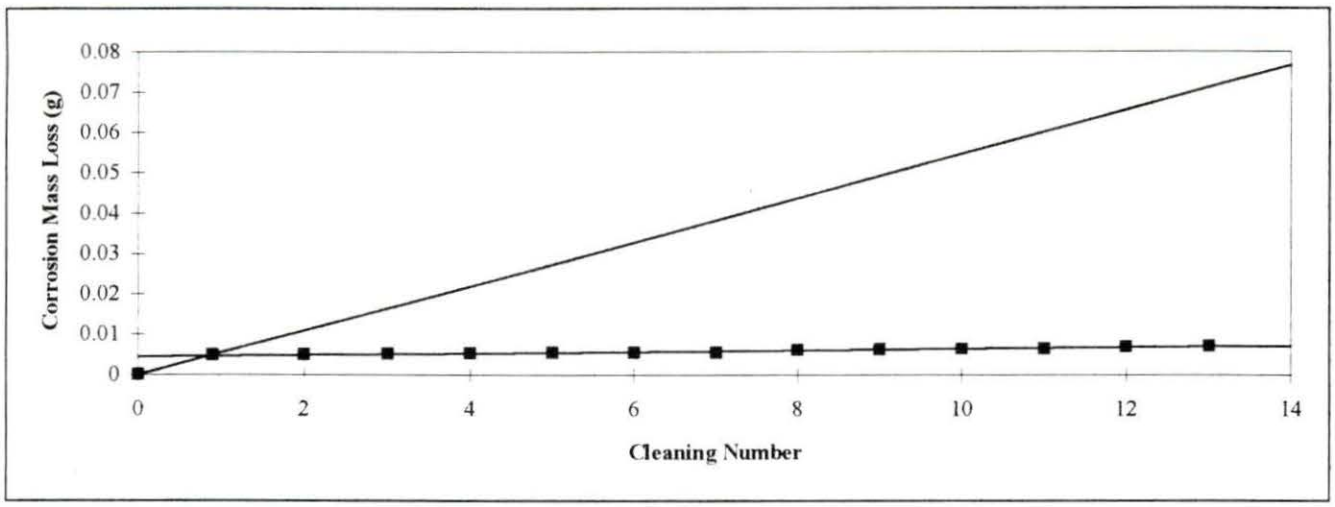

Figure A.17. Corrosion mass plot for the lying sample exposed at the low dose rate under the galvanic conditions of the combined experiments.

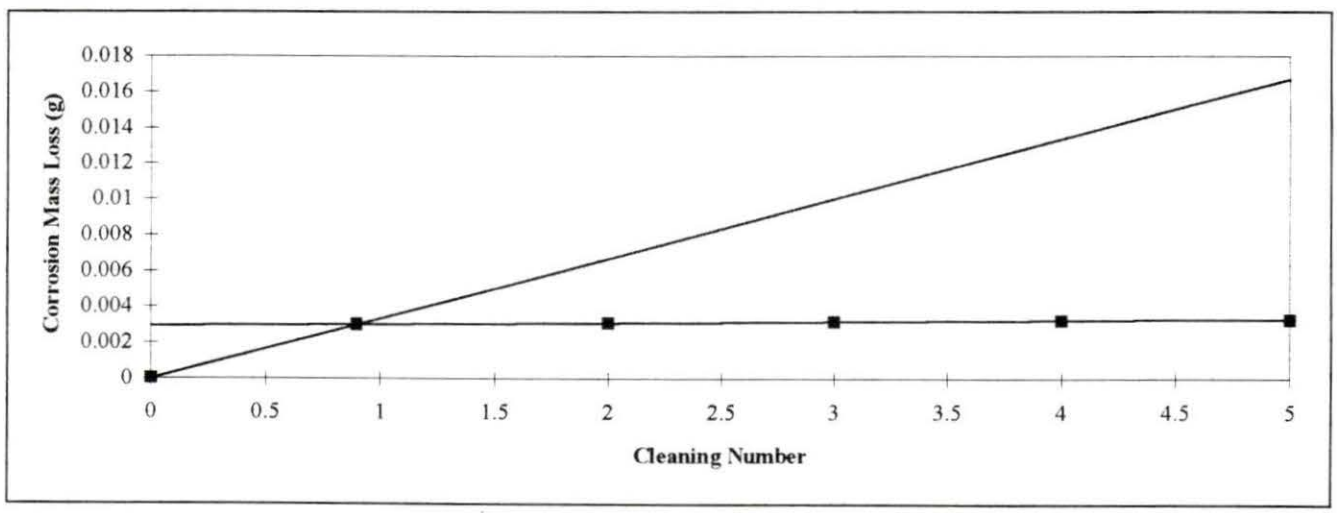

Figure A.18. Corrosion mass plot for the lying sample exposed at the low dose rate under the comparison conditions of the combined experiments.

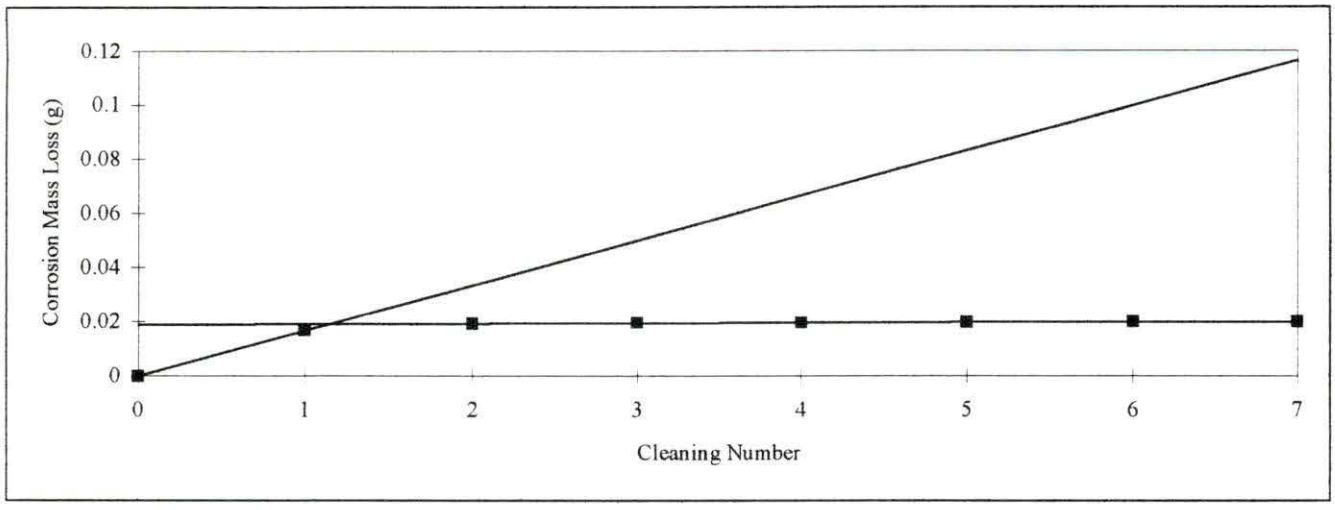

Figure A.19. Corrosion mass plot for the lying sample exposed at the high dose rate under the galvanic conditions of the combined experiments.

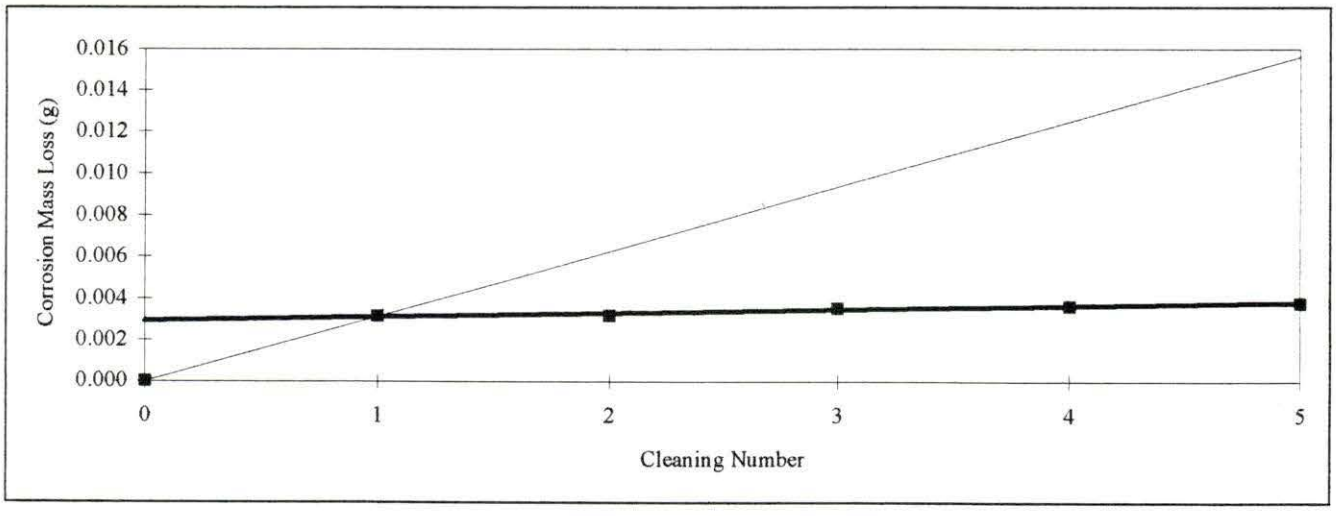

Figure A.20. Corrosion mass plot for the lying sample exposed at the high dose rate under the comparison conditions of the combined experiments.

APPENDIX B. CORROSION DATA TABLES

Table B.1. Data summary table for concrete-buffered experiments.

	Lying Samples				Hanging Samples		
Sample ID	BHL	BLL1	BLL2	BCL	BHH	BLH	BCH
Initial Mass (g)	3.665698	4.225043	4.195220	3.847130	4.078578	4.155813	3.990083
Mass (g) after Cleaning #							
0	3.660018	4.221093	4.192725	3.847036	4.078910	4.155762	3.990050
1	3.657613	4.219900	4.191886	3.846672	4.078226	4.155590	3.989878
2	3.657558	4.219816	4.191532	3.846556	4.078015	4.155520	3.989740
3	3.657500	4.219732	4.191128	3.846538	4.077854	4.155444	3.989683
4	3.657483	4.219718	4.190998	3.846444	4.077686	4.155348	3.989670
5	3.657404	4.219672	4.190924	3.846380	4.077555	4.155286	3.989590
6		4.219650	4.190945	3.846240	4.077538	4.155170	3.989554
7		4.219602	4.190932	3.846160	4.077443	4.155148	3.989550
8					4.077486		3.989417
Corrosion Mass Loss (g)	0.002412	0.001289	0.001714	0.000353	0.001138	0.000527	0.000289
Final Mass (g)	3.657606	4.219804	4.191011	3.846683	4.077772	4.155235	3.989761
Total Mass Loss (g)	0.008092	0.005239	0.004209	0.000447	0.000805	0.000578	0.000322
Surface Area (dm^2)	0.092219	0.085735	0.085735	0.093926	0.085737	0.085988	0.087413
Exposure Duration (days)	41.89722	35.05	35.05	38.26389	41.89722	35.05	38.26389
Dose Rate (rads/hr)	30414.6	6643	6643	nil	30414.6	6643	nil
Corrosion Rate[a] (mdd)	2.094264	1.743583	1.400687	0.124467	0.224163	0.191768	0.096179

[a]Corrosion Rate given in milligrams per square decimeter per day.

Table B.2. Data summary table for galvanic experiments.

	Lying Samples		Hanging Samples		
Sample ID	GHL	GCL	GHH1	GHH2	GCH
Initial Mass (g)	4.157514	4.169614	3.927186	3.989718	4.157453
Mass (g) after Cleaning #					
0	4.108675	4.115668	3.927393	3.989938	4.157575
1	4.184433	4.112930	3.926748	3.989220	4.156863
2	4.068848	4.112503	3.926613	3.989118	4.156473
3	4.068360	4.111835	3.926503	3.989135	4.156298
4	4.068296	4.111565	3.926355	3.988903	4.156143
5	4.068218	4.111543	3.926215	3.988793	4.156040
6		4.111190	3.926138	3.988630	4.155940
7			3.926095	3.988445	4.155850
8				3.988355	4.155748
9				3.988225	
Corrosion Mass Loss (g)	0.039882	0.003504	0.000675	0.000637	0.001101
Final Mass (g)	4.068793	4.112164	3.926718	3.989301	4.156474
Total Mass Loss (g)	0.088721	0.057451	0.000468	0.000417	0.000979
Contact Area (dm^2)	0.038590	0.036100	0.037565	0.037565	0.035973
Surface Area (dm^2)	0.087160	0.081852	0.085769	0.085769	0.082105
Exposure Duration (days)	28.9979	28.1125	28.9979	28.9979	28.1125
Dose Rate (rads/hr)	29476.8	nil	29476.8	29476.8	nil
Corrosion Rate[a] (mdd)	35.10303	24.96698	0.188260	0.167685	0.424044

[a]Corrosion Rate given in milligrams per square decimeter per day.

Table B.3. Data summary table for comparison experiments.

Sample ID	**Lying Sample** CCL	**Hanging Sample** CCH
Initial Mass (g)	4.620588	4.403750
Mass (g) after Cleaning #		
0	4.593420	4.403873
1	4.588418	4.403623
2	4.588303	4.403433
3	4.588088	4.403235
4	4.587970	4.402943
5	4.587875	4.402845
6	4.587725	4.402650
7		4.402483
8		4.402365
9		4.402185
Corrosion Mass Loss (g)	0.005010	0.000971
Final Mass (g)	4.588410	4.402902
Total Mass Loss (g)	0.032178	0.000848
Surface Area (dm^2)	0.094264	0.094517
Exposure Duration (days)	28.1646	28.1646
Dose Rate (rads/hr)	nil	nil
Corrosion Rate[a] (mdd)	12.12019	0.318687

[a]Corrosion Rate given in milligrams per square decimeter per day.

Table B.4. Data summary table for combined experiments.

	Galvanic Samples			Comparison Samples		
Sample ID	CGHL	CGLL	CGCL	CCHL	CCLL	CCCL
Initial Mass (g)	4.632636	4.641578	4.592120	4.556808	4.547668	4.632602
Mass (g) after Cleaning #						
0	4.574490	4.611320	4.541153	4.532090	4.526090	4.599535
1	4.557860	4.606428	4.537393	4.528970	4.523098	4.596263
2	4.555330	4.606318	4.535433	4.528950	4.522995	4.596025
3	4.554973	4.606200	4.534880	4.528600	4.522943	4.595863
4	4.555028	4.606105	4.534775	4.528490	4.522823	4.595678
5	4.554738	4.605908	4.534553	4.528340	4.522793	4.595475
6	4.554658	4.605805	4.534408			4.595285
7	4.554493	4.605718	4.534215			4.595070
8		4.605250				
9		4.605038				
10		4.604908				
11		4.604795				
12		4.604440				
13		4.604233				
Corrosion Mass Loss (g)	0.019101	0.004651	0.006009	0.003080	0.003004	0.003307
Final Mass (g)	4.555389	4.606669	4.535144	4.529010	4.523086	4.596228
Total Mass Loss (g)	0.077248	0.034909	0.056977	0.027796	0.024581	0.036374
Contact Area (dm^2)	0.041925	0.041925	0.041925	- - - -	- - - -	- - - -
Surface Area (dm^2)	0.094264	0.094264	0.094264	0.094264	0.094264	0.094264
Exposure Duration (days)	27.20208	28.22361	27.24236	27.20208	28.22361	27.24236
Dose Rate (rads/hr)	28342.6	6382.8	nil	28342.6	6382.8	nil
Corrosion Rate[a] (mdd)	30.12568	13.12148	22.18735	10.84005	9.239454	14.16434

[a]Corrosion Rate given in milligrams per square decimeter per day.

APPENDIX C. SURFACE AREA DETERMINATION PROGRAM

This Appendix contains a program written in Microsoft FORTRAN used to determine the surface area and error of the carbon steel coupons.

```
1   REAL *8 PI, LENGTH, WIDTH, LENGTHERR, WIDTHERR, EDGE1, EDGE2, EDGE
2   REAL *8 EDGE1ERR, EDGE2ERR, EDGERR, HOLE, HOLERR, ERR1, ERR2
3   REAL *8 POSHOLE, NEGHOLE, TAREA, DIAM, THICKERR, THICK
4   REAL *8 DIAMERR, TAREAERR
5   INTEGER NDIM, NHOLE
6   CHARACTER LAB*8
7   PARAMETER (THICK = .0127, THICKERR = .000127, DIAM = .0127)
8   PARAMETER (DIAMERR = .000127, PI = 3.14159265358979323846)

9   OPEN (UNIT=10, FILE='SURFAC.DAT', STATUS='NEW')

10  PRINT *, 'ENTER THE LABEL FOR THE COUPON FOR ANALYSIS'
11  READ *, LAB
12  WRITE (10,*) 'COUPON LABEL = ', LAB
13  PRINT *, 'ENTER 1 IF LYING SAMPLE AND 2 IF HANGING'
14  READ *, NHOLE
15  IF ((NHOLE.NE.1).AND.(NHOLE.NE.2)) GOTO 13

16  PRINT *, 'ENTER UNITS OF THIS COUPON (1=mm, 2=in.)'
17  READ *, NDIM
18  IF ((NDIM.NE.1).AND.(NDIM.NE.2)) GOTO 16

19  PRINT *, 'ENTER DIMENSION 1 (LENGTH)'
20  READ *, LENGTH
21  PRINT *, 'ENTER DIMENSION 2 (WIDTH)'
22  READ *, WIDTH

23  IF (NDIM.EQ.1) THEN
24      LENGTH    = LENGTH/100
25      WIDTH     = WIDTH/100
26  ELSEIF (NDIM.EQ.2) THEN
27      LENGTH    = LENGTH*.254
28      WIDTH     = WIDTH*.254
29  ENDIF
30  LENGTHERR     = LENGTH/100
31  WIDTHERR      = WIDTH/100

32  ---------SURFACE (FLAT)-------------------------
33  AREA          = LENGTH*WIDTH*2
34  AREAERR       = 2*AREA*((LENGTHERR/LENGTH)**2 + (WIDTHERR/WIDTH)**2)**.5

35  ---------EDGE-----------------------------------
36  EDGE1         = 2*THICK*WIDTH
37  EDGE1ERR      = 2*EDGE1*((THICKERR/THICK)**2+(WIDTHERR/WIDTH)**2)**.5
38  EDGE2         = 2*THICK*LENGTH
39  EDGE2ERR      = 2*EDGE2*((THICKERR/THICK)**2+(LENGTHERR/LENGTH)**2)**.5
40  EDGE          = EDGE1 + EDGE2
41  EDGERR        = (EDGE1ERR**2+EDGE2ERR**2)**.5
```

```
42    IF (NHOLE.EQ.1) THEN
43        HOLE      = 0.
44        HOLERR    = 0.
45        GOTO 56
46    ENDIF

47    ---------HOLE-----------------------------------
48    NEGHOLE       = .5*PI*DIAM**2
49    ERR1          = NEGHOLE*((DIAMERR/DIAM)**2*2)**.5
50    POSHOLE       = PI*DIAM*THICK
51    ERR2          = POSHOLE*((DIAMERR/DIAM)**2 + (THICKERR/THICK)**2)**.5
52    HOLE          = POSHOLE - NEGHOLE
53    HOLERR        = (ERR1**2+ERR2**2)**.5
54
55    ---------TOTALS & OUTPUT-------------------------
56    TAREA         = AREA + EDGE + HOLE
57    TAREAERR      = (AREAERR**2 + EDGERR**2 + HOLERR**2)**.5

58    WRITE (10,*)
59    WRITE (10,*) 'SURFACE AREA = ', TAREA
60    WRITE (10,*) 'ERROR = ', TAREAERR
61    WRITE (10,*)

62    PRINT *, 'DO YOU HAVE ANOTHER SAMPLE (1=yes, 2=no)'
63    READ *, NDIM
64    IF ((NDIM.NE.1).AND.(NDIM.NE.2)) GOTO 62

65    IF (NDIM.EQ.1) GOTO 10

66    STOP
67    END
```

APPENDIX D. ERROR ANALYSIS TABLES

Table D.1. Error analysis table for the hanging sample exposed at the control dose rate in the concrete-buffered experiments.

T-factor	=	2.571		
Residual Squared	=	11.0457		
Upper "n"	=	7		
MSE	=	8.89E-10		
Sum of Squares (x)	=	28		
Initial Mass (g)	=	3.990083	±	0.000033
C0 (g)	=	3.990050	±	0.000058
Corrosion Mass Loss (g)	=	0.000289	±	0.000095
Total Mass Loss (g)	=	0.00032	±	0.00012
Surface Area (dm^2)	=	0.0874	±	0.0022
Exposure Duration (days)	=	38.264	±	0.021
Corrosion Rate (mdd)	=	0.096	±	0.035

Table D.2. Error analysis table for the lying sample exposed at the control dose rate in the concrete-buffered experiments.

T-factor	=	2.776		
Residual Squared	=	12.4622		
Upper "n"	=	6		
MSE	=	1.12E-09		
Sum of Squares (x)	=	17.5		
Initial Mass (g)	=	3.	±	0.000042
C0 (g)	=	3.847036	±	0.000048
Corrosion Mass Loss (g)	=	0.00035	±	0.00013
Total Mass Loss (g)	=	0.00045	±	0.00014
Surface Area (dm^2)	=	0.0939	±	0.0024
Exposure Duration (days)	=	38.264	±	0.021
Corrosion Rate (mdd)	=	0.124	±	0.040

Table D.3. Error analysis table for the hanging sample exposed at the low dose rate in the concrete-buffered experiments.

T-factor	=	-----		
Residual Squared	=	-----		
Upper "n"	=	2		
MSE	=	-----		
Sum of Squares (x)	=	-----		
Initial Mass (g)	=	4.15581	±	0.00011
C0 (g)	=	4.155762	±	0.000009
Corrosion Mass Loss (g)	=	0.00053	±	0.00042
Total Mass Loss (g)	=	0.00058	±	0.00044
Surface Area (dm^2)	=	0.0860	±	0.0022
Exposure Duration (days)	=	35.050	±	0.021
Corrosion Rate (mdd)	=	0.19	±	0.15

Table D.4. Error analysis table for the first lying sample exposed at the low dose rate in the concrete-buffered experiments.

T-factor	=	3.182		
Residual Squared	=	15.3561		
Upper "n"	=	5		
MSE	=	9.74E-11		
Sum of Squares (x)	=	10		
Initial Mass (g)	=	4.225043	±	0.000049
C0 (g)	=	4.221093	±	0.000090
Corrosion Mass Loss (g)	=	0.001289	±	0.000052
Total Mass Loss (g)	=	0.00524	±	0.00011
Surface Area (dm^2)	=	0.0857	±	0.0022
Exposure Duration (days)	=	35.050	±	0.021
Corrosion Rate (mdd)	=	1.744	±	0.058

Table D.5. Error analysis table for the second lying sample exposed at the low dose rate in the concrete-buffered experiments.

T-factor	=	4.303		
Residual Squared	=	11.9510		
Upper "n"	=	4		
MSE	=	8.81E-10		
Sum of Squares (x)	=	5		
Initial Mass (g)	=	4.19522	±	0.00022
C0 (g)	=	4.192725	±	0.000069
Corrosion Mass Loss (g)	=	0.00171	±	0.00024
Total Mass Loss (g)	=	0.00421	±	0.00034
Surface Area (dm^2)	=	0.0857	±	0.0022
Exposure Duration (days)	=	35.050	±	0.021
Corrosion Rate (mdd)	=	1.40	±	0.12

Table D.6. Error analysis table for the hanging sample exposed at the high dose rate in the concrete-buffered experiments.

T-factor	=	4.303		
Residual Squared	=	23.3932		
Upper "n"	=	4		
MSE	=	1.63E-09		
Sum of Squares (x)	=	5		
Initial Mass (g)	=	4.078578	±	0.000054
C0 (g)	=	4.078910	±	0.000041
Corrosion Mass Loss (g)	=	0.00114	±	0.00042
Total Mass Loss (g)	=	0.00081	±	0.00043
Surface Area (dm^2)	=	0.0857	±	0.0021
Exposure Duration (days)	=	41.897	±	0.021
Corrosion Rate (mdd)	=	0.22	±	0.12

Table D.7. Error analysis table for the lying sample exposed at the high dose rate in the concrete-buffered experiments.

T-factor	=	4.303		
Residual Squared	=	6.3262		
Upper "n"	=	4		
MSE	=	3.16E-10		
Sum of Squares (x)	=	5		
Initial Mass (g)	=	3.665698	±	0.000052
C0 (g)	=	3.660018	±	0.000065
Corrosion Mass Loss (g)	=	0.00241	±	0.00012
Total Mass Loss (g)	=	0.00809	±	0.00015
Surface Area (dm^2)	=	0.0922	±	0.0023
Exposure Duration (days)	=	41.897	±	0.021
Corrosion Rate (mdd)	=	2.094	±	0.065

Table D.8. Error analysis table for the hanging sample exposed at the control dose rate in the galvanic experiments.

T-factor	=	2.571		
Residual Squared	=	11.9326		
Upper "n"	=	7		
MSE	=	1.35E-09		
Sum of Squares (x)	=	28		
Initial Mass (g)	=	4.15745	±	0.00015
C0 (g)	=	4.157575	±	0.000025
Corrosion Mass Loss (g)	=	0.00110	±	0.00012
Total Mass Loss (g)	=	0.00098	±	0.00019
Surface Area (dm^2)	=	0.0821	±	0.0021
Exposure Duration (days)	=	28.113	±	0.021
Corrosion Rate (mdd)	=	0.424	±	0.084

Table D.9. Error analysis table for the lying sample exposed at the control dose rate in the galvanic experiments.

T-factor	=	4.303		
Residual Squared	=	10.3681		
Upper "n"	=	4		
MSE	=	9.28E-09		
Sum of Squares (x)	=	5		
Initial Mass (g)	=	4.16961	±	0.00016
C0 (g)	=	4.115668	±	0.000046
Corrosion Mass Loss (g)	=	0.00350	±	0.00076
Total Mass Loss (g)	=	0.05745	±	0.00078
Surface Area (dm^2)	=	0.0819	±	0.0021
Exposure Duration (days)	=	28.113	±	0.021
Corrosion Rate (mdd)	=	24.97	±	0.71

Table D.10. Error analysis table for the first hanging sample exposed at the high dose rate in the galvanic experiments.

T-factor	=	2.571		
Residual Squared	=	8.7256		
Upper "n"	=	7		
MSE	=	4.18E-09		
Sum of Squares (x)	=	28		
Initial Mass (g)	=	3.92719	±	0.00015
C0 (g)	=	3.927393	±	0.000019
Corrosion Mass Loss (g)	=	0.00067	±	0.00012
Total Mass Loss (g)	=	0.00047	±	0.00019
Surface Area (dm^2)	=	0.08577	±	0.0021
Exposure Duration (days)	=	28.998	±	0.083
Corrosion Rate (mdd)	=	0.188	±	0.076

Table D.11. Error analysis table for the second hanging sample exposed at the high dose rate in the galvanic experiments.

T-factor	=	2.365		
Residual Squared	=	16.9253		
Upper "n"	=	9		
MSE	=	3.18E-09		
Sum of Squares (x)	=	60		
Initial Mass (g)	=	3.989718	±	0.000058
C0 (g)	=	3.989938	±	0.000029
Corrosion Mass Loss (g)	=	0.00064	±	0.00016
Total Mass Loss (g)	=	0.00042	±	0.00017
Surface Area (dm^2)	=	0.0858	±	0.0021
Exposure Duration (days)	=	28.998	±	0.083
Corrosion Rate (mdd)	=	0.168	±	0.069

Table D.12. Error analysis table for the lying sample exposed at the high dose rate in the galvanic experiments.

T-factor	=	4.303		
Residual Squared	=	3.4405		
Upper "n"	=	4		
MSE	=	2.58E-08		
Sum of Squares (x)	=	5		
Initial Mass (g)	=	4.157514	±	0.000092
C0 (g)	=	4.10868	±	0.00039
Corrosion Mass Loss (g)	=	0.03988	±	0.00096
Total Mass Loss (g)	=	0.0887	±	0.0010
Surface Area (dm^2)	=	0.0872	±	0.0022
Exposure Duration (days)	=	28.998	±	0.083
Corrosion Rate (mdd)	=	35.10	±	0.98

Table D.13. Error analysis table for the hanging sample exposed at the control dose rate in the comparison experiments.

T-factor	=	4.303		
Residual Squared	=	10.1141		
Upper "n"	=	4		
MSE	=	3.36E-10		
Sum of Squares (x)	=	5		
Initial Mass (g)	=	4.40375	±	0.00011
C0 (g)	=	4.403873	±	0.000063
Corrosion Mass Loss (g)	=	0.00097	±	0.00014
Total Mass Loss (g)	=	0.00085	±	0.00019
Surface Area (dm^2)	=	0.0945	±	0.0024
Exposure Duration (days)	=	28.165	±	0.021
Corrosion Rate (mdd)	=	0.319	±	0.071

Table D.14. Error analysis table for the lying sample exposed at the control dose rate in the comparison experiments.

T-factor	=	2.776		
Residual Squared	=	6.2425		
Upper "n"	=	6		
MSE	=	1.02E-09		
Sum of Squares (x)	=	17.5		
Initial Mass (g)	=	4.62059	±	0.00011
C0 (g)	=	4.59342	±	0.00014
Corrosion Mass Loss (g)	=	0.00501	±	0.00011
Total Mass Loss (g)	=	0.03218	±	0.00021
Surface Area (dm^2)	=	0.0943	±	0.0024
Exposure Duration (days)	=	28.165	±	0.021
Corrosion Rate (mdd)	=	12.12	±	0.32

Table D.15. Error analysis table for the lying sample exposed at the control dose rate under the galvanic conditions of the combined experiments.

T-factor	=	3.182		
Residual Squared	=	11.5726		
Upper "n"	=	5		
MSE	=	8.77E-10		
Sum of Squares (x)	=	10		
Initial Mass (g)	=	4.592120	±	0.000055
C0 (g)	=	4.541153	±	0.000025
Corrosion Mass Loss (g)	=	0.00601	±	0.00014
Total Mass Loss (g)	=	0.05698	±	0.00016
Surface Area (dm^2)	=	0.0943	±	0.0024
Exposure Duration (days)	=	27.242	±	0.021
Corrosion Rate (mdd)	=	22.19	±	0.56

Table D.16. Error analysis table for the lying sample exposed at the control dose rate under the comparison conditions of the combined experiments.

T-factor	=	2.571		
Residual Squared	=	8.3811		
Upper "n"	=	7		
MSE	=	2.87E-10		
Sum of Squares (x)	=	28		
Initial Mass (g)	=	4.63260	±	0.00014
C0 (g)	=	4.599535	±	0.000025
Corrosion Mass Loss (g)	=	0.003307	±	0.000052
Total Mass Loss (g)	=	0.03637	±	0.00015
Surface Area (dm^2)	=	0.0943	±	0.0024
Exposure Duration (days)	=	27.242	±	0.02083
Corrosion Rate (mdd)	=	14.16	±	0.36

Table D.17. Error analysis table for the lying sample exposed at the low dose under the galvanic conditions of the combined experiments.

T-factor	=	2.228		
Residual Squared	=	42.8933		
Upper "n"	=	12		
MSE	=	1.21E-08		
Sum of Squares (x)	=	143		
Initial Mass (g)	=	4.64158	±	0.00026
C0 (g)	=	4.611320	±	0.000066
Corrosion Mass Loss (g)	=	0.00465	±	0.00029
Total Mass Loss (g)	=	0.03491	±	0.00040
Surface Area (dm^2)	=	0.0943	±	0.0024
Exposure Duration (days)	=	28.224	±	0.021
Corrosion Rate (mdd)	=	13.12	±	0.36

Table D.18. Error analysis table for the lying sample exposed at the low dose under the comparison conditions of the combined experiments.

T-factor	=	3.182		
Residual Squared	=	3.9849		
Upper "n"	=	5		
MSE	=	5.56E-10		
Sum of Squares (x)	=	10		
Initial Mass (g)	=	4.547668	±	0.000087
C0 (g)	=	4.526090	±	0.000042
Corrosion Mass Loss (g)	=	0.003004	±	0.000095
Total Mass Loss (g)	=	0.02458	±	0.00014
Surface Area (dm^2)	=	0.0943	±	0.0024
Exposure Duration (days)	=	28.224	±	0.021
Corrosion Rate (mdd)	=	9.24	±	0.24

Table D.19. Error analysis table for the lying sample exposed at the high dose under the galvanic conditions of the combined experiments.

T-factor	=	2.776		
Residual Squared	=	11.2319		
Upper "n"	=	6		
MSE	=	8.02E-09		
Sum of Squares (x)	=	17.5		
Initial Mass (g)	=	4.63264	±	0.00015
C0 (g)	=	4.574490	±	0.000062
Corrosion Mass Loss (g)	=	0.01910	±	0.00033
Total Mass Loss (g)	=	0.07725	±	0.00037
Surface Area (dm^2)	=	0.0943	±	0.0024
Exposure Duration (days)	=	27.202	±	0.042
Corrosion Rate (mdd)	=	30.13	±	0.78

Table D.20. Error analysis table for the lying sample exposed at the high dose under the comparison conditions of the combined experiments.

T-factor	=	3.182		
Residual Squared	=	4.0606		
Upper "n"	=	5		
MSE	=	6.34E-09		
Sum of Squares (x)	=	10		
Initial Mass (g)	=	4.55681	±	0.00039
C0 (g)	=	4.532093	±	0.000074
Corrosion Mass Loss (g)	=	0.00308	±	0.00032
Total Mass Loss (g)	=	0.02780	±	0.00051
Surface Area (dm^2)	=	0.0943	±	0.0024
Exposure Duration (days)	=	27.202	±	0.042
Corrosion Rate (mdd)	=	10.84	±	0.34